Quantum Science and Technology

PAPER • **OPEN ACCESS**

Theoretical framework for quantum associative memories

To cite this article: Adrià Labay-Mora *et al* 2025 *Quantum Sci. Technol.* **10** 035050

IOP Publishing Quantum Sci. Technol. 10 (2025) 035050 https://doi.org/10.1088/2058-9565/ade184

Quantum Science and Technology

OPEN ACCESS

RECEIVED
27 August 2024

REVISED
30 May 2025

ACCEPTED FOR PUBLICATION
5 June 2025

PUBLISHED
2 July 2025

PAPER

Theoretical framework for quantum associative memories

Adrià Labay-Mora, Eliana Fiorelli, Roberta Zambrini* and Gian Luca Giorgi

Institute for Cross-Disciplinary Physics and Complex Systems (IFISC) UIB-CSIC, Campus Universitat Illes Balears, 07122 Palma de Mallorca, Spain

* Author to whom any correspondence should be addressed.

E-mail: roberta@ifisc.uib-csic.es, alabay@ifisc.uib-csic.es and gianluca@ifisc.uib-csic.es

Keywords: quantum neural networks, quantum associative memories, metastability, open quantum systems

Abstract

Associative memory (AM) refers to the ability to relate a memory with an input and targets the restoration of corrupted patterns. It has been intensively studied in classical physical systems, as in neural networks where an attractor dynamics settles on stable solutions. Several extensions to the quantum domain have been recently reported, displaying different features. In this work, we develop a comprehensive framework for a quantum AM (QAM) based on open quantum system dynamics, which allows us to compare existing models, identify the theoretical prerequisites for performing AM tasks, and extend it in different forms. The map that achieves an exponential increase in the number of stored patterns with respect to classical systems is derived. We establish the crucial role of symmetries and dissipation in the operation of QAM. Our theoretical analysis demonstrates the feasibility of addressing both quantum and classical patterns, orthogonal and non-orthogonal memories, stationary and metastable operating regimes, and measurement-based outputs. Finally, this opens up new avenues for practical applications in quantum computing and machine learning, such as quantum error correction or quantum memories.

1. Introduction

A system that is able to dynamically retrieve a set of pre-stored information can be generically referred to as associative memory (AM), a concept that has its roots in neurophysiology [1] and has been developed in the context of artificial intelligence. In 1982 a system was designed to function as an AM, the Hop-field neural network (HNN) [2]. It consists of an all-to-all network of classical spins, modeling neurons in active $(+1)$ or inactive (-1) states, evolving to minimize a certain energy function through repeated network updates. This drives the system to settle into one of many stable configurations, the one associated with a stored memory, or pattern. The HNN is indeed characterized by an attractor dynamics that enables the retrieval of a given pattern from a corrupted initial state. This features AMs as content-addressable memories, to be distinguished from random-access memory where data is accessed based on specific addresses instead of content [3]. A distinction can also be set between AMs and another common application of neural networks, such as classification. While AM focuses on retrieving patterns from distorted or incomplete inputs, classification tasks involve assigning inputs to specific categories based on learned features [4].

In the quest to enhance and extend the capabilities of AMs, quantum realizations of these systems have been proposed. Indeed, in a broader context, the success of neural networks in diverse applications—such as image and speech recognition, natural language processing, and autonomous systems—is driving innovation beyond classical settings establishing the burgeoning field of quantum machine learning [5, 6]. Recently, several different approaches have modeled quantum versions of AMs. The first proposals were reported in the nineties during the advent of quantum computing, mostly dealing with circuit-based approaches, and do not necessarily replicate the specific dynamics and functions of classical AM. Many of these digital models consist of variations of the Grover search algorithm [7–9], or quantum implementations of perceptrons [10, 11]. Digital approaches have been employed in pattern classification tasks, including particle tracks in high-energy physics [12], and genetic sequences [13]. While inspired by the classical HNN, such models cannot be regarded as proper AMs, as they lack the association property, as we will discuss later.

Besides digital models, a second and more recent approach, which we refer to as analog, explores the dynamics of (open) quantum systems for realizing quantum instances of AMs. Here, generalizations of HNNs range from two-level quantum systems to qudits, in both closed [14–16] and open quantum systems [17–20]. Some analog approaches deal with the derivation of effective AM models that exploit a quantum substrate. Examples include multimode Dicke-models [21, 22] and confocal cavities QED systems [23]. These models embed patterns via classical learning rules. Additional works focus on unleashing the storage of *quantum* patterns by exploiting quantum walks [24, 25] or single driven-dissipative resonators [26, 27].

Alongside proposing different models and implementations for quantum AM (QAM), a major motivation in this emerging field is to understand the potential advantages of using quantum mechanics in these systems, and how quantum effects can improve their performance. Some current literature contributions focus on quantifying the storage capacity, which refers to the amount of information (memories) that can be stored in a system of a given size. Among the analog models that have been proposed, many of them operate in a vanishing storage capacity regime and deal with classical patterns [17, 19, 21]. These works account for quantum effects inducing, e.g., new dynamical phases [17, 19], or speed-ups in the retrieval of information [18]. The limits of storage capacity have recently been the subject of research in a number of different models that are presented as QAM instances [20, 23, 26, 28]. Some of the proposals do not exhibit any improvement compared to the classical counterpart [20], while other instances seem to identify a potential advantage [26, 28]. Overall, this diverse collection of proposals is defining the emergent field of QAM, but a general framework that can describe and include the distinct instances of QAMs is still lacking. Consequently, performing meaningful comparisons among different models or identifying the potential of non-classical approaches remains a challenge.

The objective of this work is to develop a comprehensive theory framework for QAM, beyond existing model-specific results, by providing a unified foundation for understanding the working principles of this function. Assuming a general approach, our starting point is the set of necessary properties that a generic open quantum system must show to be regarded as an AM. This will allow us to bound the capacity of quantum states that can be stored by these kinds of systems and compare it with their classical equivalents, to frame both classical and quantum patterns, and to establish the presence of symmetries, through the definition of basins of attraction, as the enabling mechanism for QAMs. Once the operative conditions for a QAM are identified, not only one can design QAM channels to store patterns in stable states but exploit the metastable phase in open quantum systems to store transient patterns. This reformulation combines the framework developed here for stable pattern storage with the theory of classical metastability [29], allowing for faster association at the expense of ephemeral patterns.

The work is organized as follows: in section 2 we review some key points of classical and QAMs, that we employ in section 3 to provide a general definition; the result of the latter allows one to build general quantum channels, which are compatible with an AMs. An instance of such a construction is given in section 4 for both orthogonal and non-orthogonal memories. The bound to the amount of information that can be stored in a QAM is addressed in section 5. The full characterization of systems that provide QAM is addressed in sections 6 and 7, respectively discussing the role of symmetries and the alternative formulation for metastable patterns. Finally, some physical instances of AM models are revisited within the introduced framework in section 8, followed by conclusive discussion in section 9.

2. Preliminaries

In this section, we introduce some preliminary concepts and report results on the storage capacity of classical and QAMs. In the classical regime, the HNN [2] is the most paradigmatic example of a general content-addressable system endowed with a number of fixed-point attractors, as anticipated in the Introduction. Patterns are locally stable states, each of them being related to a basin of attraction, a set of states that are dynamically evolved towards the corresponding memory. A sketch can be seen in figure 1, where three fixed points encode letters that are used to correct distorted inputs. The collection of patterns is typically encoded via a learning rule in the neural connection, which, together with the dynamical evolution, characterizes the retrieval of information. These synaptic weights are chosen through a given dependency in terms of the states that serve as memories, one of the most employed being the Hebbian prescription [30]. Details about the HNN dynamics and Hebbian rule can be found in appendix A.

An important figure of merit that characterizes AMs is the *storage capacity*, defined as the maximum number of states that can be stored with respect to the size of the system,

$$\alpha = \frac{\text{maximum number of patterns}}{\text{system size}}. \tag{1}$$

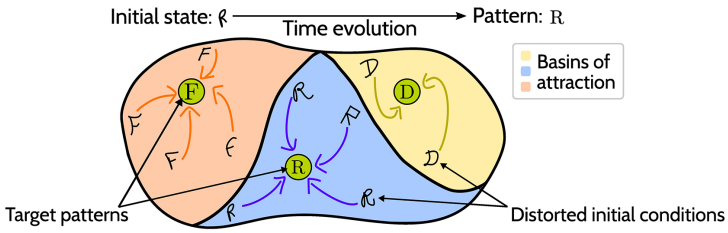

Figure 1. The phase space of a classical system powered with AM capabilities can be divided into different regions called basins of attraction. Each basin contains a stable fixed point of the dynamics, which is regarded as the pattern or memory. Then, any other initial condition belonging to the same basin will naturally converge to the corresponding pattern. Thus, the initial corrupted or distorted state is associated with the corrected version of the state, the pattern.

For each AM with a given learning rule, the corresponding storage capacity α can be derived. For instance, in a HNN consisting on n binary neurons storing M uncorrelated patterns it is defined as $\alpha = M/n$. This definition is based on the fact that classical patterns are stored as binary strings of length n, in which one can define at most n orthogonal vectors. Then, if such patterns are encoded using the Hebbian prescription, the storage capacity has been shown to have a limiting value of $\alpha^{\text{Hebb}} = 0.138$ [31]. When considering other learning rules, such as, e.g. the pseudo-inverse learning rule [32] or nonlinear interactions [33], the corresponding limiting value α can increase, e.g. reaching $n/\ln n^2$ in the case of correlated patterns [34].

The problem of storage capacity has been posed in more general terms in the seminal works of E. Gardner [35, 36]. Here, a set of patterns is imposed to be stationary states, while leaving the learning rule as a free parameter. As a result, a bound is found on the maximum value that the storage capacity can take for an entire class of HNN-type AMs, i.e. irrespective of the specific learning prescription. Such a bound is often referred to as a *critical* storage capacity, and denoted as α_c, to distinguish it from the storage capacity α calculated when a learning rule is defined. In Gardner's approach, the critical storage capacity of a HNN is analyzed as a function of both the degree of pattern correlation and the size of the basin of attraction. In the limit of uncorrelated patterns and vanishing basin of attraction, the critical storage capacity reads $\alpha_c^{\text{HNN}} = 2$, decreasing when enlarging the basin of attraction, and increasing when permitting correlated patterns [35].

Concerning the issue of quantifying the storage capacity of QAM looking for a possible quantum advantage, two main directions have been followed. Several research contributions tackle specific instances of QAM. In this case, some results point out possible improvements with respect to the Hebbian limit [23, 26], while other platforms are shown to behave similarly or worse than classical instances [20]. Alternatively, recent contributions aim to provide more general bounds on the critical storage capacity of QAMs [20, 28]. In these scenarios, and in the same spirit of Gardner's program, one can define a quantum system undergoing retrieval dynamics while leaving the learning rule as a free parameter. In this respect, [28] shows that a quantum neural network behaving as a QAM can outperform the critical capacity of classical counterparts when renouncing any basin of attraction.

As previously stated, establishing the extent of the applicability of the aforementioned outcomes remains a challenge, as a theoretical framework must still be defined. This is required to support both patterns as quantum states, similar to [27, 28], as well as memories exhibiting finite basins of attraction [20, 21]. Tackling such an issue can allow us to shed light on (i) the general form of a QAM, and advance on the question as to whether the (ii) the critical storage capacity of the latter can outperform the classical AM.

In the two following sections, we combine the general approach that exploits the evolution of an open quantum system, as introduced in [28], with Hopfield's original idea [2] of dynamical systems displaying finite basin of attractions for each pattern. With these tools, we will tackle the issue (i) and (ii), to characterize the properties and form of a completely positive trace-preserving (CPTP) channel for QAM. Moreover, we will compute the storage capacity for different scenarios, particularly distinguishing the tasks where the retrieval of information is done with or without a measurement.

3. Theoretical framework

To address the limitations of current approaches and build a comprehensive theory, we start by framing the original definition of AM [2] into the quantum formalism. Here, the pure (mixed) states of a physical system are represented by elements of a Hilbert space $\mathcal{H}$ ($\mathcal{B}(\mathcal{H})$ space of bounded linear operators on $\mathcal{H}$), and the dynamical evolution is described through a quantum channel, say Λ. This general formulation allows us to

identify which properties and limitations characterize a generic (open) quantum system with $(\mathcal{H}, \Lambda)$, that can be regarded as a QAM. Although we will first focus on the case of stable memories, we will see in section 7 that the conditions imposed are also satisfied for metastable patterns.

Quantum maps or channels are a key tool for describing the dynamics of quantum systems. They can be employed to formalize the continuous dynamics of open quantum systems undergoing Markovian evolution [37, 38], as well as discrete operations in quantum computation. Examples include noise effects, several types of qubit errors, and measurement processes [39]. In general, a quantum channel Λ is an operator that transforms a state $\hat{\rho} \in \mathcal{B}(\mathcal{H})$ into another state $\Lambda(\hat{\rho}) = \hat{\rho}'$, where $\hat{\rho}' \in \mathcal{B}(\mathcal{H}')$ [40], the simplest example being a unitary evolution, $\Lambda(\hat{\rho}) = \hat{U}\hat{\rho}\hat{U}^\dagger$. The evolution of a state $\hat{\rho} \in \mathcal{B}(\mathcal{H})$ by means of a CPTP map reads

$$\Lambda(\hat{\rho}) = \sum_{\alpha=1}^{t} \hat{K}_\alpha \hat{\rho} \hat{K}_\alpha^\dagger, \tag{2}$$

where $t \leqslant (\dim \mathcal{H})^2$, and $\{\hat{K}_\alpha\}$ represents a set of Kraus operators, satisfying [41]

$$\sum_{\alpha=1}^{t} \hat{K}_\alpha^\dagger \hat{K}_\alpha = \mathbb{I}. \tag{3}$$

With the above definitions, we now identify the key properties and conditions that a quantum system with $(\mathcal{H}, \Lambda)$ must possess to function as a QAM.

As we anticipated, a classical AM requires a particular set of states to be stable fixed points of the dynamics. This guarantees that states representing the correct patterns are left unchanged by the dynamics and no information is lost (we will see a generalization in terms of metastable states in section 7). We thus require that (**condition C1**) the set of M states representing the patterns, $\{\hat{\rho}_\mu \in \mathcal{B}(\mathcal{H})\}_{\mu=1}^{M}$, are fixed points of the CPTP map [37, 42, 43]

$$\Lambda(\hat{\rho}_\mu) = \hat{\rho}_\mu, \qquad \mu = 1, \ldots, M. \tag{4}$$

For CPTP maps acting on finite-dimensional Hilbert spaces, condition (4) admits at least one solution [44] where maps with just one fixed point are said to be ergodic [45]. The existence of multiple fixed points has been extensively studied in the literature for both finite [46] and infinite dimensional cases [47]. Of course, any convex combination of these states is also a fixed point, an occurrence that we will further comment on at the end of the section (see equation (7)). To encompass the most general case of multiple fixed points, we may introduce the notion of maximal invariant subspace, $\mathcal{S}$, that, loosely speaking, represents the largest collection of states within the Hilbert space that remains unchanged under the action of the map. More precisely, given a state $\hat{\rho}$ with support $\mathrm{supp}(\hat{\rho}) \subset \mathcal{S}$, then $\mathrm{supp}[\Lambda(\hat{\rho})] \subset \mathcal{S}$, where $\mathrm{supp}(X)$ is the set of eigenvectors of X orthogonal to its kernel (i.e. with non-vanishing eigenvalues). As a note, eigenstates of unitary maps do not represent patterns as defined in equation (4), except for the trivial identity map.

Secondly, we introduce the concept of decaying space $\mathcal{D}$, that encompasses all quantum states $|\omega\rangle$ whose evolution under (many r) repeated actions of Λ vanishes in $\mathcal{D}$, i.e. $\mathcal{D} = \left\{ |\varphi\rangle \in \mathcal{H} \mid \langle\varphi|\Lambda^r(\rho)|\varphi\rangle \underset{r\to\infty}{\longrightarrow} 0 \right.$ $\left.\text{for any } \rho \in \mathcal{B}(\mathcal{H}) \right\}$ [46, 47]. In other words, the states in the decaying subspace are mapped through Λ into a state in the stable subspace. For a QAM to function, we need the invariant subspace $\mathcal{S}$ to be attractive: either a state belongs to it or is mapped towards it via the evolution, the decaying subspace being thus complementary to the stable subspace, $\mathcal{D} = \mathcal{S}^\perp$. It is worth noticing that the decomposition of the Hilbert space into a stable subspace $\mathcal{S}$, containing the patterns, and a decaying subspace $\mathcal{D}$, containing the classification information is not general. Indeed, it can be proven to hold true for CPTP maps in the Markovian case [48], if $\dim \mathcal{H} < \infty$, which need to be attractive [49] if $\dim \mathcal{H} = \infty$ [46, 50]. For generic CPTP maps with an invariant subspace $\mathcal{S}$, the above restriction on the Hilbert space decomposition is satisfied by Kraus operators that take the form [51]

$$\hat{K}_\alpha = \left(\begin{array}{c|c} K_\alpha^{\mathrm{S}} & K_\alpha^{\mathrm{SD}} \\ \hline 0 & K_\alpha^{\mathrm{D}} \end{array}\right). \tag{5}$$

Here, K_α^{S} (K_α^{D}) evolves the state in the invariant (decaying) subspace, and K_α^{SD} plays the role of mapping the states from the decaying subspace into the stable one. We will refer to this term as cross-term. Importantly, the zero block in the lower-left corner ensures that no information escapes from the stable state space.

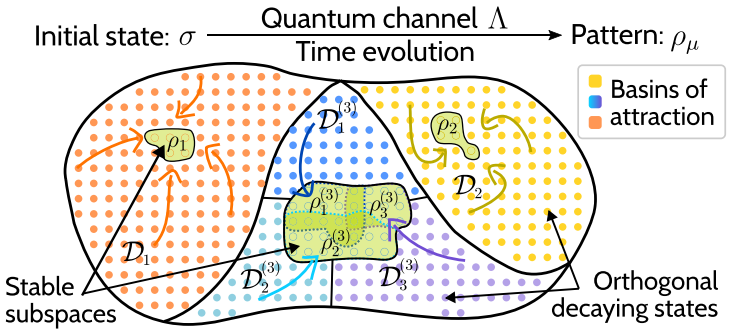

Figure 2. Quantum model for AM. The points represent the elements in a basis of the Hilbert space $\mathcal{H}$, and the quantum states $\hat{\rho}_\mu$ represent the patterns to be stored. Here, $\hat{\rho}_1$ and $\hat{\rho}_2$ are orthogonal patterns while the states $\hat{\rho}_\ell^{(3)}$ represent non-orthogonal patterns. The figure highlights the division of the Hilbert space into decaying subspaces $\mathcal{D}_\mu$, containing the initial conditions that converge towards the corresponding pattern.

Condition C1 is necessary but not sufficient for a QAM as we require that a sub-collection of states in $\mathcal{D}$ are associated with a particular pattern $\hat{\rho}_\mu$. To this end, we require that **(condition C2)** for each fixed point $\hat{\rho}_\mu$ there exists a region of the Hilbert space, $\mathcal{D}_\mu$ (decaying space), enclosing all the states that converge to the corresponding fixed point, $\hat{\rho}_\mu$, under the action of the map Λ (see figure 2). Then, analogous to the classical basin of attraction depicted in figure 1, the quantum basin of attraction of a given fixed point is the combined set of the decaying space and the fixed point itself, as we will write explicitly in the next section. We stress the importance of modeling the presence of non-vanishing decaying spaces. Indeed, this feature excludes the trivial identity map from QAM and identifies the association property of the AM. We further note that beyond classical AM, its necessity is also recognized in (open) quantum systems performing quantum state classification tasks [24, 52, 53].

Finally, we enforce that **(condition C3)** any two states from different decaying spaces cannot be associated with the same memory $\hat{\rho}_\mu$. To this end, we prevent the regions $\{\mathcal{D}_\mu\}$ from sharing common states, by requiring their mutual disjointness. A way to impose the latter is actually dealing with mutual orthogonal spaces (see definition (1)) [54]. Although it may appear restrictive, we will see that this condition is fulfilled in physical quantum systems, like, e.g. those displaying symmetries [55–57], as well as classical systems with multiple stable fixed points [58]. As we will see, this condition permits perfect association between a state and its closest pattern, while non-ideal situations exhibiting mixed decaying subspaces generally lead to imperfect QAM [59].

In summary, a quantum system with $(\mathcal{H}, \Lambda)$ can function as a QAM if it meets the following requirements: (C1) patterns are quantum states $\hat{\rho}_\mu$ that are fixed points of the map Λ as in equation (4); (C2) for each pattern $\hat{\rho}_\mu$ there exists a non-vanishing decaying space, $\mathcal{D}_\mu$; and (C3) the decaying spaces are mutually disjoint.

We can now formally define the necessary ingredients for a QAM as follows:

Definition 1. A system with Hilbert space $\mathcal{H}$, and CPTP map Λ functions as a QAM if there exists a set of M fixed point of the map $\{\hat{\rho}_\mu \in \mathcal{B}(\mathcal{H})\}_{\mu=1}^M$, each one associated with a non-empty decaying subspace $\mathcal{D}_\mu \subset \mathcal{D}$, with $\mathcal{D}$ the total decaying subspace, orthogonal to the maximal invariant one, $\mathcal{D} = \mathcal{S}^\perp$. The subspaces $\mathcal{D}_\mu$ are orthogonal one another, $\mathcal{D}_\mu \perp \mathcal{D}_\nu \; \forall \mu \neq \nu$, and

$$\lim_{r\to\infty} \Lambda^r(\hat{\sigma}) = \hat{\rho}_\mu \qquad \forall \hat{\sigma} \in \mathcal{B}(\mathcal{D}_\mu)\,. \tag{6}$$

As commented before, each decaying subspace $\mathcal{D}_\mu$ has a non-vanishing dimension, $\dim \mathcal{D}_\mu = d_\mu > 0 \; \forall \mu$, so each memory pattern can be reached from at least one decaying state. Moreover, since we imposed disjointness on the decaying spaces, $\mathcal{D}_\mu \cap \mathcal{D}_\nu$ is trivial $\forall \mu \neq \nu$, the evolution does not allow states from different basins to mix [54]. It also follows, from the disjointness of the decaying spaces, that the total decaying subspace $\mathcal{D}$ is the direct sum of the individual decaying subspaces $\mathcal{D}_\mu$: $\mathcal{D} = \bigoplus_{\mu=1}^M \mathcal{D}_\mu$; where M is the number of fixed points.

Although definition 1 shares similarities with its classical counterpart, it is worth noticing that there is a fundamental difference between the two descriptions. While a classical HNN evolves towards its local stable states through nonlinear dynamics, the dynamics of a quantum system is inherently linear due to the fundamental principles of quantum mechanics [6]. As a consequence, given a QAM as defined above, any

classical mixture of the set of patterns is also left unchanged by the action of the map. For instance, if we take two memory states $\hat{\rho}_\mu$ and $\hat{\rho}_\nu$, their classical mixture $p\hat{\rho}_\mu + (1-p)\hat{\rho}_\nu$ is an invariant state, as it is

$$\Lambda\left[p\hat{\rho}_\mu + (1-p)\,\hat{\rho}_\nu\right] = p\hat{\rho}_\mu + (1-p)\,\hat{\rho}_\nu. \tag{7}$$

Moreover, it is straightforward to see that each of the classical mixtures can be related to a new corresponding basin of attraction. Referring to the above example, any state belonging to $\mathcal{D}_\mu \oplus \mathcal{D}_\nu$ is associated with a classical mixture of the respective patterns. As a result, for a QAM obeying the definition 1, and displaying a set of M patterns, any classical mixture of the latter behaves as an additional stable fixed point. By adopting the nomenclature employed in classical associative memories, classical mixtures of patterns can be referred to as *spurious* memories—states that are local minima but do not belong to the family of patterns. It is worth noticing that, even though classical AM models as the HNN exhibit spurious patterns [30], this occurrence is not systematic. Only certain combinations of classical patterns, and only in certain parametric regimes, will behave as stable fixed points of the dynamics. This is instead a common feature of all QAM and we will discuss how this potential limitation can be handled in section 4.

We also point out a distinctive capability of QAM that does not have any classical counterpart. Depending on the tasks that one delineates for the patterns upon retrieval, a QAM can support either a quantum output or a classical one. The first one refers to any set of (combination of) patterns that is retrieved by the QAM and does not require any further process, in this sense consisting of a quantum output. Suppose instead that one needs to access classical information. In that case, a measurement process can be further performed, leading to a probabilistic result of the patterns that matched the initial state. The measurement process may be seen as a nonlinear activation function which may produce an incorrect output [10]. However, the possibility of repeating the process a statistically significant number of times leads to additional information about the nature of the initial state, such as its similarity not only to the closest pattern but also to the rest of the patterns [60]. We will comment on the differences between quantum and classical outputs in section 5, where we will study the storage capacity properties of quantum associative memories.

4. Quantum maps for AM

In this section, we provide an explicit construction of a quantum channel Λ to realize a QAM according to definition 1 and discuss how a learning rule emerges in this formalism. For pedagogical reasons, we divide the analysis into two parts. First, in section 4.1, we build a map storing $M_\perp$ orthogonal quantum states $\{\hat{\rho}_\mu\}$ as fixed points; this is in analogy to classical models which require nearly orthogonal patterns for error-free retrieval [2]. Then, in section 4.2 we consider a more general problem where besides storing $M_\perp$ orthogonal patterns $\{\hat{\rho}_\mu\}$, we also allow for the storage of $M_{\not\perp}$ non-orthogonal quantum patterns $\{\hat{\rho}_\ell\}$. Hence, we demonstrate how a quantum formulation of AM can store arbitrary quantum states as patterns without restriction on the dimension of the stable subspace. It is important to specify that in this section, we are able to derive maps fulfilling the QAM as in definition 1, upon some further restrictions. Hence, other maps may exist that store the same patterns. The notation introduced in this section is summarized in table 1 for reference.

4.1. Orthogonal patterns

Let us consider the finite-dimensional Hilbert space $\mathcal{H}$ with $\dim\mathcal{H} = N$, and let $\{\hat{\rho}_\mu \in \mathcal{B}(\mathcal{H})\}_{\mu=1}^{M}$ be the $M = M_\perp$ orthogonal patterns. We will then set the conditions under which definition 1 can be met. That is, consistently with the general discussion of section 3, the space requires an orthogonal decomposition into stable and decaying parts such that $\mathcal{H} = \mathcal{S} \oplus \mathcal{D}$ where the decaying part can be further decomposed into M orthogonal blocks $\{\mathcal{D}_\mu\}_{\mu=1}^{M}$ (one for each pattern). Similarly, the stable subspace must be further decomposed into M orthogonal blocks $\{\mathcal{S}_\mu\}_{\mu=1}^{M}$ where each $\mathcal{S}_\mu$ is the support of the pattern $\hat{\rho}_\mu$, $\mathcal{S}_\mu = \mathrm{supp}(\hat{\rho}_\mu)$ [46, 47]. These subspaces give rise to the maximal invariant subspace as $\mathcal{S} = \bigoplus_\mu \mathcal{S}_\mu \subset \mathcal{H}$ where $\dim\mathcal{S}_\mu = s_\mu \geqslant 1$ and $\dim\mathcal{S} = \sum_\mu s_\mu = N^{\mathrm{S}} < N$ the corresponding dimensions. The complementary part of the Hilbert space which is not preserved by the map spans the decaying subspace of dimension $\dim\mathcal{D} = N - N^{\mathrm{S}} = N^{\mathrm{D}}$, where the dimension of each block is $d_\mu = \dim\mathcal{D}_\mu$. Then, due to the orthogonality between blocks in both stable and decaying parts, we can define the basins of attraction for each pattern as $\mathcal{H}_\mu = \mathcal{S}_\mu \oplus \mathcal{D}_\mu$ such that $\mathcal{H} = \bigoplus_{\mu=1}^{M} \mathcal{H}_\mu$.

In our scenario, we want to guarantee that the association of a set of states to a specific pattern, say $\hat{\rho}_\mu$, only occurs within subspaces corresponding to the same label μ. As such, also the Kraus operators need to display a block structure, $\hat{K}_\alpha = \bigoplus_\mu \hat{K}_{\alpha,\mu}$, where each one of the block $\hat{K}_{\alpha,\mu}$ has the form defined by

Table 1. Notation.

Symbol	Definition
$\mathcal{H}$	Complete Hilbert space
$\mathcal{B}(\bullet)$	Space of bounded linear operators on $\bullet$
$\mathcal{S}/\mathcal{D}$	Stable/decaying subspace of $\mathcal{H}$
$N^{\mathrm{S}}/N^{\mathrm{D}}$	Dimension of stable/decaying subspace
N	Total Hilbert space dimension
$\mathcal{S}_\mu$	Irreducible stable subspace
$\mathcal{X}_\tau$	Decoherence-free subspace (DFS)
$C_\perp/C_\not\perp$	Number of irreducible/decoherence-free subspaces
$\hat{\rho}_\mu$	Orthogonal pattern spanning $\mathcal{S}_\mu$
$\hat{\rho}_\ell^{(\tau)}$	Non-orthogonal pattern in $\mathcal{X}_\tau$
$M_\perp/M_\not\perp$	Number of orthogonal/non-orthogonal patterns
$m_\not\perp^{(\tau)}$	Number of non-orthogonal patterns in $\mathcal{X}_\tau$
M	Total number of patterns
$\mathcal{D}_\mu/\mathcal{D}_\ell^{(\tau)}$	Decaying subspace of pattern $\hat{\rho}_\mu/\hat{\rho}_\ell^{(\tau)}$
s_μ/s_τ	Dimension of $\mathcal{S}_\mu/\mathcal{X}_\tau$
$d_\mu/d_\ell^{(\tau)}$	Dimension of $\mathcal{D}_\mu/\mathcal{D}_\ell^{(\tau)}$
$\mathcal{H}_\mu/\mathcal{H}_\ell^{(\tau)}$	Basin of attraction of $\hat{\rho}_\mu/\hat{\rho}_\ell^{(\tau)}$
$\lvert\mu_j\rangle/\lvert\tau_j\rangle$	jth basis element of $\mathcal{S}_\mu/\mathcal{X}_\tau$
$\lvert\omega_x^{(\mu)}\rangle/\lvert\omega_x^{(\tau,\ell)}\rangle$	xth basis element of $\mathcal{D}_\mu/\mathcal{D}_\ell^{(\tau)}$

equation (5). Consequently, the map Λ, when restricted to the subspace $\mathcal{H}_\mu$, has a unique fixed point $\hat{\rho}_\mu$ [61]. Thus, the operators $\hat{K}_{\alpha,\mu}$ must leave invariant the μth subspace $\mathcal{S}_\mu$, i.e. $\hat{K}_{\alpha,\mu}\mathcal{S}_\mu \subseteq \mathcal{S}_\mu$ [37, 45]. In order to continue building the map we impose the commutation relation $[\hat{K}_{\alpha,\mu}, \hat{\rho}_\mu] = 0\ \forall\alpha$ to ensure that the patterns are fixed points of Λ [37, 43]. We will also assume the Kraus operators $\hat{K}_{\alpha,\mu}$ to be diagonalizable. Moreover, the map further restricted to the stable subspace $\mathcal{S}_\mu$ contains a unique, full-rank fixed point, $\hat{\rho}_\mu$, and it can be shown that $[K^{\mathrm{S}}_{\alpha,\mu}, \hat{\rho}_\mu] = 0$ [51]. Hence, $\hat{\rho}_\mu$ and the operators $K^{\mathrm{S}}_{\alpha,\mu}$ can be simultaneously diagonalized with respect to the same basis of eigenvectors, say $\{|\mu_j\rangle\}_{j=1}^{s_\mu}$. In this basis, it is $\hat{\rho}_\mu = \sum_{j=1}^{s_\mu} u_j^\mu |\mu_j\rangle\langle\mu_j|$, and we write for the operator on the stable subspace

$$K^{\mathrm{S}}_{\alpha,\mu} = \sum_{j=1}^{s_\mu} a^\alpha_{\mu,j} |\mu_j\rangle\langle\mu_j|. \tag{8}$$

This constrains each Kraus operator $K^{\mathrm{S}}_{\alpha,\mu}$ to the form of the pattern state.

Let us now focus on the part of the Kraus operators $\hat{K}_{\alpha,\mu}$ acting on the decaying subspace, which we called $K^{\mathrm{D}}_{\alpha,\mu}$. Reminding that $\mathcal{D}_\mu \perp \mathcal{S}_\mu$, and without loss of generality, we identify with $\{|\omega_j^\mu\rangle\}_j, j = 1, \ldots, d_\mu$, the orthonormal basis of $\mathcal{D}_\mu$ in which $K^{\mathrm{D}}_{\alpha,\mu}$ can be diagonalized,

$$K^{\mathrm{D}}_{\alpha,\mu} = \sum_{x=1}^{d_\mu} c^\alpha_{\mu,x} |\omega_x^\mu\rangle\langle\omega_x^\mu|. \tag{9}$$

It is worth noticing the label μ for states $|\omega_j^\mu\rangle$, which highlights that any state $\hat{\sigma}$ belonging to the μth decaying subspace, $\hat{\sigma} \in \mathcal{B}(\mathcal{D}_\mu)$, is associated to the corresponding stable subspace $\mathcal{S}_\mu$ through equation (6). Finally, the cross-term $\hat{K}^{\mathrm{SD}}_{\alpha,\mu}$ must map any state from the decaying subspace $\mathcal{D}_\mu$ to the stable one, $\mathcal{S}_\mu$. That is, it needs to satisfy $K^{\mathrm{SD}}_{\alpha,\mu}\mathcal{D}_\mu \subset \mathcal{S}_\mu$. Therefore, referring to the basis $\{|\omega_x^\mu\rangle\}$ and $\{|\mu_j\rangle\}$, the most general expression for the cross-term reads

$$K^{\mathrm{SD}}_{\alpha,\mu} = \sum_{j=1}^{s_\mu}\sum_{x=1}^{d_\mu} b^\alpha_{\mu,j,x} |\mu_j\rangle\langle\omega_x^\mu|. \tag{10}$$

For equations (8)–(10) to define a proper set of Kraus operators, we need to impose that any density operator, under the action of the map Λ, is evolved into a likewise valid density operator. Thus, the CPTP condition defined by equation (3) must hold. Leaving the details of the derivation in appendix B, we get

$$\sum_\alpha |a^\alpha_{\mu,j}|^2 = 1, \tag{11a}$$

$$\sum_{\alpha}\left(a^{\alpha}_{\mu,j}\right)^{*} b^{\alpha}_{\mu,j,x}=0, \tag{11b}$$

$$\sum_{\alpha}\left[\sum_{j=1}^{s_\mu}\left(b^{\alpha}_{\mu,j,y}\right)^{*} b^{\alpha}_{\mu,j,x}\right]+\delta_{xy}|c^{\alpha}_{\mu,x}|^2=\delta_{xy}, \tag{11c}$$

which represent a series of constraints for the coefficients of equations (8)–(10).

As a last step, it is worth noting that the form of the Kraus operators presented describes a system whose dynamics converge to a set of multiple steady states. However, the steady states are not uniquely defined as any state diagonal in the basis of $K^{\mathrm{S}}_{\alpha,\mu}$ is also a fixed point of the map. For this reason, we need to enforce the associativity condition (6) for a specific set of states $\{\hat{\rho}_\mu\}_{\mu=1}^{M}$, corresponding to the patterns. Hence, to guarantee that the states of the decaying subspace $\mathcal{D}_\mu$ evolve to the corresponding pattern, $\hat{\rho}_\mu$, the cross-term must satisfy

$$\sum_{\alpha} K^{\mathrm{SD}}_{\alpha}|\omega^{\mu}_{x}\rangle\langle\omega^{\mu}_{y}|\left(K^{\mathrm{SD}}_{\alpha}\right)^{\dagger}=\kappa^{\mu}_{xy}\hat{\rho}_\mu, \tag{12}$$

where the constant κ^{μ}_{xy} determines the rate at which the operator $|\omega^{\mu}_{x}\rangle\langle\omega^{\mu}_{y}|$ converges to the pattern $\hat{\rho}_\mu$.

The three conditions defined by equation (11*a*)–(11*c*), together with equation (12), determine the *learning rule* which allows one to construct the CPTP map ruling a QAM with the quantum patterns $\{\hat{\rho}_\mu\}_{\mu=1}^{M}$. In appendix C.1, we continue the derivation of the Kraus operators by determining the value of the parameters in relation to the quantum patterns.

The CPTP map Λ derived in this section enables an AM mechanism. This can be compared with [28] where a complete basis of the Hilbert space is assumed to be a set of fixed points of the map. However, imposing such a strict bound on the number of patterns implies no decaying space, i.e. the basins of attraction are reduced to the same memories. It is then concluded that the CPTP map realizing the association acts as a genuine incoherent operation [62], i.e. as a decoherence map taking any quantum state to its classical mixture [63]. It is possible to show that the map Λ that we derived reduces to the one obtained in [28], upon restricting Λ itself to the stable subspace (see appendix D for details on the derivation). Moreover, our generalization permits us to endow each pattern with a finite-dimensional set of states that decay all and solely to the pattern itself. Any initial state displaying components in different basins of attraction will asymptotically evolve towards a convex superposition of patterns. However, the presence of finite-dimensional and disjoint decaying subspaces, $\mathcal{D}_\mu$, permits the occurrence of pure association to one and only one pattern $\hat{\rho}_\mu$.

Example 1. *Local amplitude damping*. To illustrate the concepts introduced so far, let us consider a simple example based on a modified amplitude damping channel acting on the subspace spanned by the pattern $|\mu\rangle$ and the decaying state $|\omega_\mu\rangle$. The Kraus operators of the map in such basis are $\hat{K}_{0,\mu}=a^{0}_{\mu}|\mu\rangle\langle\mu|+\sqrt{1-q_\mu}|\omega_\mu\rangle\langle\omega_\mu|$, $\hat{K}_{1,\mu}=a^{1}_{\mu}|\mu\rangle\langle\mu|$, and $\hat{K}_{2,\mu}=\sqrt{q_\mu}|\mu\rangle\langle\omega_\mu|$ where $q_\mu\in[0,1)$, $\sum_\alpha|a^{\alpha}_{\mu}|^2=1$, and $a^{\alpha}_{\mu}\neq a^{\alpha}_{\nu}$ if $\mu\neq\nu$ (in such a way the Kraus operators are not proportional to the identity). Then, the complete Kraus operators are given by $\hat{K}_\alpha=\bigoplus_\mu\hat{K}_{\alpha,\mu}$. Here, a state $\hat{\sigma}^{(0)}=\sum_{\mu,\nu}x_{\mu\nu}|\mu\rangle\langle\nu|+y_{\mu\nu}|\omega_\mu\rangle\langle\omega_\nu|+z_{\mu\nu}|\mu\rangle\langle\omega_\nu|+z^{*}_{\mu\nu}|\omega_\mu\rangle\langle\nu|$ transforms, under the action of the map, as

$$\begin{aligned}
x_{\mu\nu}&\to\left[\sum_{\alpha}\left(a^{\alpha}_{\mu}\right)^{*}a^{\alpha}_{\nu}\right]x_{\mu\nu}+\sqrt{q_\mu q_\nu}y_{\mu\nu},\\
y_{\mu\nu}&\to y_{\mu\nu}\sqrt{(1-q_\mu)(1-q_\nu)},\\
z_{\mu\nu}&\to a^{0}_{\mu}\sqrt{1-q_\nu}z_{\mu\nu}.
\end{aligned}$$

Thus, in the limit of infinite applications of the map, the state $\hat{\sigma}^{(0)}$ is evolved toward the state $\hat{\sigma}^{(\infty)}=\sum_\mu(x_{\mu\mu}+y_{\mu\mu})|\mu\rangle\langle\mu|$. This demonstrates the associative nature of the map since the contribution of the decaying states $y_{\mu\mu}$ is driven towards the respective pattern. At the same time, the off-diagonal terms do not affect the outcome. Since they represent transitions between different basins of attraction (i.e. between different patterns $|\mu\rangle$ and $|\nu\rangle$), their presence is transient during the evolution. Still, they vanish in the limit of infinite applications of the map.

Beyond exhibiting the associative mechanism, the above example is also illustrative of the limitations exposed in section 3. Indeed, the map leaves not only the intended memory patterns but also any convex combination of them (i.e. their mixtures) unchanged. As already commented, this occurrence can be considered the quantum equivalent of a spurious memory, a stable state that is not in the family of patterns.

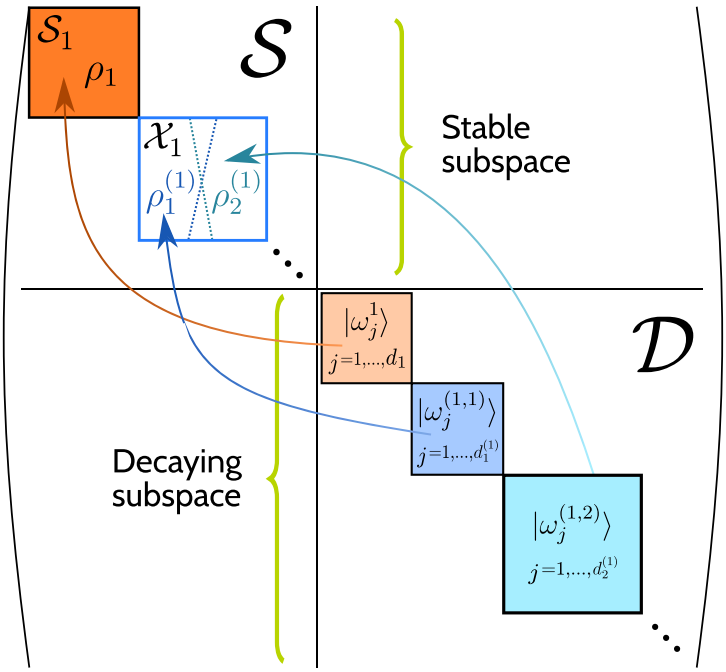

Figure 3. Action on quantum states of the most general form of the QAM map Λ capable of storing orthogonal and non-orthogonal quantum patterns. Each orthogonal block in the stable subspace may correspond to an irreducible subspace $\mathcal{S}_\mu = \text{supp}(\hat{\rho}_\mu)$ or a decoherence-free subspace such that $\{\hat{\rho}_\ell^{(\tau)} \in \mathcal{B}(\mathcal{X}_\tau)\}_\ell$. The orthogonality of the states in the decaying subspace guarantees perfect association under the evolution of the map Λ (represented by the arrows).

To overcome the presence of spurious memories in QAM, a potential strategy can be devised by leveraging quantum measurements as follows. In the case of orthogonal patterns, one can always define a projective measurement, $\{\hat{P}_\mu\}_{\mu=1}^M$, such that $\text{tr}\,\hat{P}_\mu\hat{\rho}_\nu = \delta_{\mu\nu}$. Then let us assume that an initial, corrupted state $\hat{\sigma}^{(0)}$ whose probability to be found in a state corresponding to the pattern μ is $p_\mu^{(0)} = \text{tr}\,\hat{P}_\mu\hat{\sigma}^{(0)} = x_{\mu\mu}$. Via multiple applications of the map, the state $\hat{\sigma}^{(0)}$ has been associated with a final, spurious state whose probability to be found in the pattern μ is $p_\mu^{(\infty)} = \text{tr}\,\hat{P}_\mu\hat{\sigma}^{(\infty)} = x_{\mu\mu} + y_{\mu\mu} > p_\mu^{(0)}$. Therefore, performing the quantum measurement will yield, with high probability, the pattern μ^* that best overlaps with the final state $\hat{\sigma}^{(\infty)}$, up to a failure probability that depends on the contribution of the other patterns in the initial state.

4.2. General formulation

In the previous section, we developed a quantum channel Λ allowing the storage of states with orthogonal support. In the following, we extend such analysis to the case of a QAM displaying general quantum states as patterns, thus including those with non-orthogonal support. Hence, we want to first identify the structure of the Hilbert space allowing for storage of $M_\perp$ orthogonal $\{\hat{\rho}_\mu\}$ ($\text{supp}(\hat{\rho}_\mu)\cap\text{supp}(\hat{\rho}_\nu) = \emptyset\,\forall\mu,\nu$) and $M_\not\perp$ non-orthogonal patterns $\{\hat{\rho}_\ell\}$ ($\text{supp}(\hat{\rho}_\ell)\cap\text{supp}(\hat{\rho}_{\ell'}) \neq \emptyset$ for some ℓ,ℓ') to subsequently construct the CPTP map realizing the association.

Consistently with definition 1, the structure of the Hilbert space is again divided into two orthogonal blocks, $\mathcal{S}$ and $\mathcal{D} = \mathcal{S}^\perp$, representing the invariant subspace and the decaying one, respectively. With respect to the former, there appear $M_\perp$ fixed points of the map $\{\hat{\rho}_\mu\}_{\mu=1}^{M_\perp}$, each of them spanning irreducible and orthogonal supports $\mathcal{S}_\mu$. In addition, we aim at storing $M_\not\perp$ non-orthogonal patterns $\{\hat{\rho}_\ell\}$ for which we divide into orthogonal sets say $\{\hat{\rho}_\ell^{(\tau)} \in \mathcal{B}(\mathcal{X}_\tau)\}_{\ell=1}^{m_\not\perp^{(\tau)}}$. Hence, in order to consider the most general partition, we assume $\hat{\rho}_\ell^{(\tau)} \perp \hat{\rho}_\ell^{(\tau')}$ if they belong to different sets $\tau \neq \tau'$ but those in the same set are not orthogonal, i.e. $\text{supp}(\hat{\rho}_\ell^{(\tau)})\cap\text{supp}(\hat{\rho}_{\ell'}^{(\tau)})\ \forall\ell,\ell'$ is not trivial. As such, notice that the total number of non-orthogonal patterns read $M_\not\perp = \sum_{\tau=1}^{C_\not\perp} m_\not\perp^{(\tau)}$ given $m_\not\perp^{(\tau)}$ non-orthogonal patterns in the τth set. The storage of such patterns requires the addition of $C_\not\perp$ subspaces, $\mathcal{X}_\tau$, each one preserving the coherences between their minimal invariant states, which hence exhibit non-orthogonal supports. In this general scenario, the decomposition of the invariant subspace reads [46, 47]

$$\mathcal{S} = \bigoplus_{\mu=1}^{M_\perp}\mathcal{S}_\mu \oplus \bigoplus_{\tau=1}^{C_\not\perp}\mathcal{X}_\tau, \tag{13}$$

where both $\mathcal{S}_\mu$, $\mu = 1,\ldots,M_\perp$ and $\mathcal{X}_\tau$, $\tau = 1,\ldots,C_\not\perp$ are all mutually orthogonal subspaces [46, 47, 64]. For the sake of completeness, we also add that each subspace $\mathcal{X}_\tau$ can be in turn decomposed in terms of orthogonal subspaces, $\mathcal{X}_\tau = \bigoplus_j \mathcal{W}_{j,\tau}$. However, such a decomposition is not unique: there exists an isomorphism, $\mathcal{U}_\tau$, mapping a given decomposition $\mathcal{W}_{j,\tau}$ to an equivalent one, $\mathcal{W}'_{j,\tau}$, and thus relating all the minimal invariant states in $\mathcal{X}_\tau$ one another. This, in turn, yields, in the most general case, subsystems in $\mathcal{X}_\tau$ that are free from decoherence [46, 47]. In particular, any decomposition of $\mathcal{X}_\tau$ in terms of 1-dimensional $\mathcal{W}_{j,\tau}$ corresponds to a decoherence-free subspace (DFS), whereas any decomposition in terms of at least 2-dimensional $\mathcal{W}_{j,\tau}$ corresponds to a noiseless subsystem. In the following, we will focus on the DFS case, and the non-unique decomposition in terms of the subspaces $\mathcal{W}_{j,\tau}$ will play no role. It is worth also stressing that any other coherence, e.g. between $\mathcal{S}_\mu$ and $\mathcal{X}_\tau$, as well as between any two of either $\mathcal{S}_\mu$ and $\mathcal{S}_{\mu'}$, or $\mathcal{X}_\tau$ and $\mathcal{X}_{\tau'}$ is not preserved by the evolution. For the sake of clarity, we write explicitly the full decomposition of the Hilbert space, $\mathcal{H} = \bigoplus_{\mu=1}^{M_\perp}(\mathcal{S}_\mu \oplus \mathcal{D}_\mu)\bigoplus_{\tau=1}^{C_\not\perp}(\mathcal{X}_\tau \oplus \mathcal{D}_\tau)$.

The presence of non-orthogonal patterns requires a more general definition of the QAM map Λ. The Kraus operators can be decomposed as $\hat{K}_\alpha = \bigoplus_{\mu=1}^{M_\perp}\hat{K}_{\alpha,\mu}\bigoplus_{\tau=1}^{C_\not\perp}\hat{K}_{\alpha,\tau}$. Here, the first part of the operators $\{\hat{K}_{\alpha,\mu}\}_{\mu=1}^{M_\perp}$ act on the related subspace $\bigoplus_{\mu=1}^{M_\perp}\mathcal{S}_\mu \oplus \mathcal{D}_\mu$, so the results derived in section 4.1 can be directly applied. The remaining part, $\{\hat{K}_{\alpha,\tau}\}_{\tau=1}^{C_\not\perp}$, needs to be slightly reformulated to permit the storage of a given set of non-orthogonal patterns. Indeed, let us focus on the subspace $\mathcal{X}_\tau$, with $\dim\mathcal{X}_\tau = s_\tau$, and let $\{|\tau_j\rangle\}_{j=1}^{s_\tau}$ be a basis of such a space. It is worth noticing that, as we deal with DFS, each $\mathcal{X}_\tau$ preserves any quantum state that can be written in a basis of the subspace. As a consequence, so long as there exists a non-empty decaying subspace $\mathcal{D}_\tau$, and no other properties are enforced, any state belonging to $\mathcal{X}_\tau$ behaves as a pattern. Nonetheless, we aim at storing the *specific* set of fixed points $\{\hat{\rho}_\ell^{(\tau)} \in \mathcal{B}(\mathcal{X}_\tau)\}_{\ell=1}^{m_\not\perp^{(\tau)}}$ for $\tau = 1,\ldots,C_\not\perp$. Accordingly, a more detailed structure of the decaying subspace $\mathcal{D}_\tau$ needs to be defined.

In order to store the collection of fixed points $\hat{\rho}_\ell^{(\tau)}$, $\ell = 1,\ldots,m_\not\perp^{(\tau)}$, which are in general neither orthogonal nor linearly independent, we associate, to each one of them, a decaying subspace $\mathcal{D}_\ell^{(\tau)} = \mathrm{span}\{|\omega_x^{(\tau,\ell)}\rangle\}_{x=1}^{d_\ell^{(\tau)}}$. The states $\{|\omega_x^{(\tau,\ell)}\rangle\}_{x=1}^{d_\ell}$ form an orthonormal basis, which is orthogonal to the stable subspace, consistently with definition 1. As a result, we can write the τth decaying space through a block structure,

$$\mathcal{D}_\tau = \bigoplus_{\ell=1}^{m_\not\perp^{(\tau)}}\mathcal{D}_\ell^{(\tau)}. \tag{14}$$

Hence, the most general expression for the Kraus operators acting on $\mathcal{X}_\tau \oplus \mathcal{D}_\tau$ is again given in terms of a block structure, as defined by equation (5). The three main blocks, $\hat{K}^{\mathrm{S}}_{\alpha,\tau}$, $\hat{K}^{\mathrm{D}}_{\alpha,\tau}$, which act on $\mathcal{X}_\tau$, $\mathcal{D}_\tau$, respectively, and the mixing one, $\hat{K}^{\mathrm{SD}}_{\alpha,\tau}$, can be tackled separately.

Let us consider first the Kraus operator acting on the stable subspace. Here, because coherences between elements of the basis, $|\tau_j\rangle\langle\tau_j|\tau_k$, are preserved, and given that we impose the fixed point condition defined by equation (4), the operator is proportional to the identity [51]

$$K^{\mathrm{S}}_{\alpha,\tau} = a^\alpha_\tau \mathbb{I}_\tau. \tag{15}$$

The coefficients a^α_τ need to satisfy the CPTP conditions (11*a*), so it holds that $\sum_\alpha |a^\alpha_\tau|^2 = 1$.

The Kraus operator acting on the decaying subspace $\mathcal{D}_\tau$ can be further reduced. Indeed, given the decomposition in equation (14), it is $K^{\mathrm{D}}_{\alpha,\tau} = \bigoplus_{\ell=1}^{m_\not\perp^{(\tau)}} K^{\mathrm{D}}_{\alpha,\tau,\ell}$, where

$$K^{\mathrm{D}}_{\alpha,\tau,\ell} = \sum_{x=1}^{d_\ell^{(\tau)}} c^{\alpha,\tau}_{\ell,x}|\omega_x^{(\tau,\ell)}\rangle\langle\omega_x^{(\tau,\ell)}|. \tag{16}$$

Finally, we focus on the mixing term, $\hat{K}^{\mathrm{SD}}_{\alpha,\tau}$, which plays a key role as it maps states belonging to the subspace $\mathcal{D}_\ell^{(\tau)}$ into the corresponding pattern $\hat{\rho}_\ell^{(\tau)}$. In general, we can write

$$K^{\mathrm{SD}}_{\alpha,\tau} = \sum_{\ell=1}^{m_\not\perp^{(\tau)}}\sum_{j=1}^{s_\tau}\sum_{x=1}^{d_\ell^{(\tau)}} b^{\alpha,\tau}_{\ell,j,x}|\tau_j\rangle\langle\omega_x^{(\tau,\ell)}|, \tag{17}$$

which needs to satisfy the associativity condition

$$\sum_\alpha K^{\mathrm{SD}}_\alpha|\omega_x^{(\tau,\ell)}\rangle\langle\,\omega_y^{(\tau,\ell')}|\left(K^{\mathrm{SD}}_\alpha\right)^\dagger = \delta_{\ell\ell'}\kappa^\ell_{xy}\hat{\rho}_\ell^{(\tau)}. \tag{18}$$

We note that, in comparison to equation (12) an additional delta function appears. This guarantees that cross-terms belonging to different decaying subspaces are suppressed and do not evolve to stable states different from the patterns. In case the quantum patterns can be expressed as pure states, i.e. $\hat{\rho}_\ell = |\psi_\ell\rangle\langle\psi_\ell|$, then it is possible to find an expression for the Kraus parameters in equations (15)–(17) as can be seen in appendix C.2.

5. Storage capacity

As anticipated in section 2, an important quantity that characterizes AMs is the storage capacity introduced in equation (1). This expression can be interpreted as the density of states that an AM can faithfully store. In the quantum realm, one would like to store quantum states and subsequently quantify how many of them can be accommodated by a QAM. Here, in analogy with the number of classical orthogonal vectors that define the space of possible patterns, a meaningful quantity to consider is the Hilbert space dimension quantifying the number of possible orthogonal states of the system. For instance, a network of n qubits features a 2^n-dimensional Hilbert space. However, as we will see, not all of them can be simultaneously stored due to the restrictions imposed in definition 1. This value, 2^n, serves as a fundamental limit on the storage capacity of a QAM based on n qubits.

More in general, a N-dimensional Hilbert space admits N orthogonal states. Hence, the most natural generalization of equation (1) defining the storage capacity of a QAM is

$$\alpha^{\mathrm{Q}} = \frac{M}{\dim \mathcal{H}}, \tag{19}$$

where M identifies the number of stored patterns. Similarly to the classical case, analyzing the storage capacity of a QAM amounts to determining the maximum number of patterns that can be faithfully stored. The advantage of this definition lies in its universality for any finite-dimensional quantum system, as it remains independent of the number of constituent units. In contrast, classical definitions of storage capacity are typically tied to specific models, such as HNNs, where the capacity is often defined in terms of the number of neurons [2]. Alternative formulations, based on the number of synapses [65] or more recent approaches with different activation functions [54], show that such definitions lack general applicability. For this reason, the definition proposed here seeks to overcome these limitations by providing a model-independent framework suitable for comparisons between quantum systems. However, meaningful comparisons between classical and quantum memories must account for differences in pattern encoding and system scaling.

Before going ahead, let us remark that, as already mentioned at the end of section 3, we can devise two different kinds of QAM tasks, leading to different definitions of storage capacities: (i) in the first case, that we identify as quantum output, we ask the computation to give the requested quantum pattern ($\hat{\rho}_\mu$) as a direct output, which is not measured at any stage. This approach is suitable for applications where the retrieved quantum information needs to be manipulated or processed further using quantum operations; and (ii) in the second scenario, corresponding to a classical output being related to the quantum state that undergoes a measurement process. The outcome of this measurement is the projected state with a probability depending on the overlap with the corresponding memory. Measurements lead to the identification of the label (μ) associated with the basin of attraction as it would also occur in classification tasks. We stress that the distinctive feature in (ii) is the presence of measurement, while the entire retrieval process, including the evolution map, is ruled by quantum dynamics [6].

We also note that this distinction is independent of the form of the patterns, which can still be generic quantum states. In the following, we will analyze the critical storage capacity of a QAM for both scenarios. We remind (see section 2) that the maximum storage capacity depends on the given learning rule [31–33] and it is upper-bounded by the optimal or critical storage capacity, which is instead independent of the specific learning prescription [35, 36].

5.1. Quantum output

We will now focus on retrieved states that are regarded as quantum outputs. In this case, let us first consider the critical storage capacity when restricting to orthogonal patterns. The result is contained in the following:

Theorem 1. *The critical storage capacity of a quantum associative memory storing a set of orthogonal patterns is* $\alpha_c^{\mathrm{Q},\perp} = 1/2$, *and it is saturated by rank-1 patterns,* $\hat{\rho}_\mu = |\psi_\mu\rangle\langle\psi_\mu|$.

Proof. For each pattern, we enforce a non-empty decaying subspace. Furthermore, since we want to store the maximum number of patterns with finite basins of attraction, we set $d_\mu = 1$ (the smallest non-vanishing decaying subspace with one element). At this point, a condition that allows one to exploit all the stable subspace for storing patterns consists of taking the minimum rank for each pattern, setting $s_\mu = 1$. This in turn implies

$\hat{\rho}_\mu = |\psi_\mu\rangle\langle\psi_\mu|$. Collecting the above results, the number of stored patterns is $M = N^{\mathrm{S}} = N^{\mathrm{D}}$, and the Hilbert space dimension is $N = N^{\mathrm{S}} + N^{\mathrm{D}}$. Thus, by employing equation (19), it is $\alpha_c^{\mathrm{Q},\perp} = (N/2)/N = 1/2$. □

The criticality of this bound can be understood as follows. Attempting to store more than $N/2$ orthogonal patterns would result in insufficient decaying states for each pattern, and the additional patterns would have no associated basin. Therefore, the extra memory becomes unreachable unless the initial state perfectly matches the desired pattern. Conversely, removing a pattern would create a spurious state in the stable subspace, i.e. a state that remains invariant under the dynamics but is not a memory. In this case, more information could be stored without increasing the dimension of the system.

Our formulation establishes a significant advantage in terms of storage capacity compared to classical associative memories. Going back to the network of n qubits of Hilbert space dimension 2^n, its critical capacity corresponds to 2^{n-1} patterns, which exponentially outperforms classical models. Through a general formulation, we derived (in the previous section) a CPTP map displaying this exponential storage capacity and also presenting finite basins of attraction. We notice that this map improves the capacity $2^{n/2}$ of other QAM analysis with finite basins of attraction [28].

Beyond orthogonal patterns, we also construct a map (see in section 4.2) that enables storing an arbitrary number of non-orthogonal states in DFSs. However, this does not imply an infinite storage capacity. The reason is that, by requiring a non-empty basin of attraction for each non-orthogonal pattern, we obtain a larger Hilbert space dimension only as a result of an increasing decaying part. On the contrary, in the orthogonal case, the addition of a pattern requires a larger dimension for both the stable and the decaying subspace.

In the most general case (see section 4.2) we have $M_\perp$ ($M_{\not\perp}$) orthogonal (non-orthogonal) patterns stored in a stable subspace of dimension N^{S}, which we can divide into $N^{\mathrm{S}}_\perp + N^{\mathrm{S}}_{\not\perp}$. Note that $N^{\mathrm{S}}_{\not\perp}$ is independent of the number of non-orthogonal patterns, while $N^{\mathrm{S}}_\perp$ grows at least linearly with $M_\perp$. Instead, the dimension of the decaying subspace N^{D} grows for each memory (independent of its type), so that the storage capacity is

$$\alpha^{\mathrm{Q}} = \frac{M_\perp + M_{\not\perp}}{N^{\mathrm{S}} + N^{\mathrm{D}}} = \frac{M_\perp + M_{\not\perp}}{N^{\mathrm{S}}_\perp(M_\perp) + N^{\mathrm{S}}_{\not\perp} + N^{\mathrm{D}}(M)}. \tag{20}$$

Then, taking into account theorem 1 and assuming $N^{\mathrm{D}} \sim \mathcal{O}(M)$, the critical storage capacity is

$$\alpha_c^{\mathrm{Q}} \sim \frac{M_\perp + M_{\not\perp}}{2M_\perp + M_{\not\perp}}. \tag{21}$$

As an example, let us consider a stable subspace consisting of only one DFS, $\mathcal{S} = \mathcal{X}$, with $\dim\mathcal{S} = N^{\mathrm{S}}_{\not\perp} = N^{\mathrm{S}}$. The storage of $M = M_{\not\perp}$ patterns requires a finite-dimensional decaying subspace that is at least M-dimensional. Since only the dimension of the decaying subspace needs to increase, the storage capacity is $M/(M + N^{\mathrm{S}})$, which converges to a critical storage capacity of 1 in the limit of $M \to \infty$.

5.2. Classical output

An AM can be used to perform classification tasks for which it is necessary to obtain information about the state at the end of the process. Hence, a measurement of the final quantum state must be performed to determine the pattern. As anticipated in section 3, due to the phenomenology of measurements in quantum mechanics, one has to repeat the process with multiple copies of the initial state. The resulting statistics provide information on the similarity between the different patterns. This, in turn, allows one to identify which memory is most similar to the final state (as in the classical case), and to gain information on how close the input state was compared to other patterns. This situation is relevant when taking into account non-orthogonal quantum patterns (see section 4.2), which cannot be perfectly discriminated [66, 67]. As a result, this occurrence impacts the storage capacity of a QAM when employed to retrieve classical information.

We aim to assess the effect of measurement on the storage capacity for the case outlined above. To this end, let us consider the general case in which patterns are given by $M_\perp$ orthogonal quantum states $\{\hat{\rho}_\mu\}$, and $M_{\not\perp}$ non-orthogonal quantum states $\{\hat{\rho}_\ell\}$, with $\mathrm{tr}(\hat{\rho}_\mu\hat{\rho}_\ell) = 0\ \forall\mu,\ell$. For the first ones, there exists a projective measurement $\hat{P}^\perp_\mu$, such that $\mathrm{tr}\,\hat{P}^\perp_\mu\hat{\rho}_\nu = \delta_{\mu\nu}$, perfectly discriminating the orthogonal states. Instead, for the non-orthogonal states, any measurement displays a finite error probability P_{err} [68]. Although several techniques exist that minimize the discrimination error, these depend on the particular states to be distinguished [69, 70]. In general, we will assume that for the set of non-orthogonal patterns $\{\hat{\rho}_\ell\}$, an optimal positive operator valued measure can be found, with a given success probability for discriminating

non-orthogonal states, $P_{\text{succ}}^{\text{opt}} = 1 - P_{\text{err}}^{\text{opt}} < 1$. Then, following equation (21), the storage capacity becomes

$$\alpha_c^{\text{QC}} \sim \frac{M_\perp + P_{\text{succ}}^{\text{opt}} M_\not\perp}{2M_\perp + M_\not\perp}. \tag{22}$$

In the limit $M_\not\perp \to \infty$, the success probability vanishes, as it is not possible to discriminate an infinite number of quantum states within a finite-dimensional state space. In addition, notice that $\alpha_c^{\text{QC}} < \alpha_c^{\text{Q}}$, and for any sub-optimal measure we will have $\alpha^{\text{QC}} < \alpha_c^{\text{QC}}$. This result is consistent with the fact that, when dealing with non-orthogonal patterns, the amount of information stored is smaller than in the orthogonal scenario as a result of patterns being correlated. This occurrence is also highlighted in the classical scenarios when considering correlated patterns [35], and it has been recently introduced in a continuous-variable system, where the memories are not necessarily orthogonal [26].

Example 2. *Storage capacity with DFS.* Consider an AM with patterns being M geometrically uniform states (GUS), $|\psi_\mu\rangle = \hat{U}^{\mu-1}|\psi\rangle$, $\mu = 1,\ldots,M$, where $\hat{U}$ is a unitary operator satisfying $\hat{U}^M = \mathbb{I}_S$ and the patterns are in general not orthogonal (with $M_\not\perp = M$). Without loss of generality, the decaying subspace is set to contain M orthogonal states $\{|\omega_\mu\rangle\}_{\mu=1}^M$, each associated with the corresponding pattern $|\psi_\mu\rangle$. In section 8.3 we show that we can indeed construct the channel that realizes the association between states in the decaying subspace with the corresponding pattern. Therefore, following equation (20), the storage capacity for such a map is $\alpha^{\text{Q}} = M/(N^{\text{S}} + M)$, where N^{S} is the dimension of the stable subspace. When increasing the number of patterns, the dimension of the stable subspace remains constant. Thus, in the limit $M \to \infty$ we get a finite storage capacity, $\alpha_c^{\text{Q}} \to 1$. Instead, when including a measurement process, we need to account for the maximum success probability of discriminating GUS. This can be written as $P_{\text{succ}}^{\text{opt}} = N^{\text{S}}/M$, by using the so-called square-root measurement [71, 72]. Therefore, the resulting storage capacity vanishes when increasing the number of patterns, i.e. it is $\alpha_c^{\text{QC}} = P_{\text{succ}}^{\text{opt}} \alpha^{\text{Q}} = N^{\text{S}}/(N^{\text{S}} + M) \to 0$ as $M \to \infty$.

6. Symmetries enabling QAM

This section explores systems that can be used as quantum associative memories, providing both the patterns and a learning rule. In particular, we discuss how memories can be encoded in steady states of a given open system that exhibits symmetry.

First of all, to enforce the presence of quantum memories, we consider systems that admit multiple steady states, or, equivalently, multiple conserved quantities. This occurrence alone does not provide any insight into the size and shape of decaying spaces $\mathcal{D}_\mu$, and thus, on basins of attraction. A sufficient condition for the Hilbert space to separate in invariant subspaces, and related decaying ones is the additional appearance of certain types of symmetries, as we illustrate below. Before going ahead, we point out that there are some differences between how symmetries emerge in Lindbladian open quantum systems and generic CPTP maps. As such, in the following, we will address both scenarios.

Let us start considering an open quantum system evolving in a Markovian fashion, as described by the Gorini–Kossakowski–Sudarshan–Lindblad (GKSL) equation [38]

$$\dot{\hat{\rho}} = \mathcal{L}\hat{\rho} = -\mathrm{i}\left[\hat{H}, \hat{\rho}\right] + \sum_\ell \hat{F}_\ell \hat{\rho} \hat{F}_\ell^\dagger - \frac{1}{2}\{\hat{F}_\ell^\dagger \hat{F}_\ell, \hat{\rho}\}.$$

Here, the Liouvillian $\mathcal{L}$ is the generator of the quantum map, $\hat{H}$ is the Hamiltonian of the system, and $\hat{F}_\ell$ are the so-called jump operators. The system admits multiple steady states if the eigenspace of eigenvalue zero of the Liouvillian, say $\mathcal{L}_{\text{ss}}$, is multi-dimensional. The maximum dimension of this eigenspace is N^2, where $N = \dim(\mathcal{H})$. Notably, while all steady states are elements of $\mathcal{L}_{\text{ss}}$, the contrary is, in general, not true [56]. Before proceeding further, it is convenient to recall that the evolution of a generic operator $\hat{O}$ reads $\dot{\hat{O}} = \mathcal{L}^\dagger(\hat{O}) = \mathrm{i}[\hat{H}, \hat{O}] + \sum_\ell \hat{F}_\ell^\dagger \hat{O} \hat{F}_\ell - \frac{1}{2}\{\hat{F}_\ell^\dagger \hat{F}_\ell, \hat{O}\}$, where $\mathcal{L}^\dagger$ is the adjoint of the Liouvillian with respect to trace norm.

In this scenario, if the system displays a strong symmetry, we can make use of the steady states as quantum memories and, additionally, identify the basins of attraction. Indeed, in a strong symmetry, by definition, there exists a number, say M, of operators $\hat{J}_\mu$ that commute with both the Hamiltonian $\hat{H}$ and the jump operators $\hat{F}_\ell$. If the latter condition holds true, then $\{\hat{J}_\mu\}_{\mu=1}^M$ is a set of conserved quantities, $\dot{\hat{J}}_\mu = 0 \forall \mu$, and, equivalently, the stationary space $\mathcal{L}_{\text{ss}}$ is M-dimensional. Moreover, a strong symmetry also induces a weak one (where $\hat{J}_\mu$ commute with $\mathcal{L}$) [55, 56], thus allowing one to separate the Hilbert space in symmetry sectors, $\mathcal{H} = \bigoplus_\mu \mathcal{H}_\mu$. Notably, the evolution inside each μth space is split from the others.

If the M conserved quantities are orthogonal projectors onto the subspace $\mathcal{H}_\mu$, the stationary space $\mathcal{L}_{\text{ss}}$ does not contain coherences, and each of the subspaces $\mathcal{H}_\mu$ hosts a stationary state, which plays the role of

the memory. With respect to the notation employed in section 4, we can thus identify $\mathcal{S}_\mu$, the support of the μth stationary state, as well as its corresponding decaying subspace $\mathcal{D}_\mu$ as the orthogonal complement of $\mathcal{S}_\mu$ with respect to $\mathcal{H}_\mu$. In the most general situation, the stationary space $\mathcal{L}_{\rm ss}$ also contains steady state coherences [56]. In this case, the structure of the stationary state is more complex, as it can host DFSs and noiseless subsystems, which have been introduced in section 4.

It is worth remarking that there are cases where a set of M conserved quantities, $\hat{J}_\mu$, does not correspond to any symmetry [56]. These are referred to as dynamical symmetries. Here, both the emergence of the latter and the identification of the decaying space have to be carried out on a case-by-case basis.

Let us now consider the case of a generic CPTP map Λ. At variance with the previous Markovian case, to derive a separation of the Hilbert space in symmetry sectors, we need to restrict to conserved orthogonal projectors. Indeed, on the one hand, this guarantees multiple steady states, and, on the other hand, it ensures the presence of a global symmetry of the map and of a Hilbert space decomposition. For a more detailed discussion on symmetries and CPTP maps see, e.g. [51]. For our purpose, the following is sufficient:

Proposition 1. *Orthogonal projectors $\hat{J}_\mu$ are conserved quantities, $\Lambda^\dagger(\hat{J}_\mu)=\hat{J}_\mu$, iff they commute with the Kraus operators $[\hat{J}_\mu,\hat{K}_\alpha]=0$, $\forall\alpha,\mu$.*

Proof. To demonstrate the above result, we proceed similarly to the case of generic conserved quantities (see, e.g. theorem 5(ii) in [73]). For the sake of a lighter notation, we drop the index μ in the following. If $[\hat{J},\hat{K}_\alpha]=0$ then $\Lambda^\dagger(\hat{J})=\sum_\alpha \hat{K}_\alpha^\dagger J\hat{K}_\alpha=\hat{J}(\sum_\alpha \hat{K}_\alpha^\dagger\hat{K}_\alpha)=\hat{J}$. Conversely, let us assume $\Lambda^\dagger(\hat{J})=\hat{J}$. It can be shown that the following relation holds,

$$\sum_\alpha \left[\hat{J},\hat{K}_\alpha\right]^\dagger\left[\hat{J},\hat{K}_\alpha\right]=\Lambda^\dagger\left[\hat{J}^\dagger\hat{J}\right]-\hat{J}^\dagger\hat{J}.$$

The right-hand side of the above expression vanishes, as $\hat{J}^\dagger\hat{J}=\hat{J}$, $\hat{J}$ being a conserved quantity by assumption; the left-hand side is a sum of positive semidefinite quantities, vanishing iff $[\hat{J},\hat{K}_\alpha]=0$. □

As a consequence of the above Proposition, the set $\hat{J}_\mu$ forms an algebra of matrices, which in turn induces a block decomposition of the Hilbert space $\mathcal{H}$. Each state $\hat{\rho}\in\mathcal{B}(\mathcal{H})$ can be thus decomposed as a block matrix, the evolution inside each block being separate. It is worth stressing that the conservation of the projectors, (i.e. their commutation with the Kraus operators), also implies the invariance of the CPTP map under $\hat{J}_\mu$, $\hat{J}_\mu\Lambda(\hat{\rho})\hat{J}_\mu^\dagger=\Lambda(\hat{J}_\mu\hat{\rho}\hat{J}_\mu^\dagger)$, in analogy with a weak symmetry for a Markovian system. In the case $\hat{J}_\mu$ being generic conserved quantities, the above results are restricted to the maximal invariant subspace $\mathcal{S}$. It can indeed be shown that the Kraus operators $K_\alpha^{\mathcal{S}}$ commute with the components $\hat{P}_S\hat{J}_\mu\hat{P}_S$, $\hat{P}_S$ identifying the projector on $\mathcal{S}$. Hence, the block structure identified through the algebra of matrix of $\hat{P}_S\hat{J}_\mu\hat{P}_S$ pertains to the subspace $\mathcal{S}$ only. As a consequence, the identification of the decaying subspace is not straightforward, in analogy with the case of a dynamical symmetry in the Markovian case.

7. Framework for metastable patterns

All the previous discussion is based on the use of memories encoded into steady states. However, recently, the possibility of realizing a QAM in a metastable regime has been shown [26, 27]. This transient memory can speed up retrieval because the decay to the metastable patterns occurs on a shorter timescale than the steady state decay. Therefore, tasks that do not require long-term memory can benefit from this approach. In this section we address this alternative scenario that will be also illustrated in section 8.2.1.

In general, the evolution of a state that undergoes a GKSL equation can be decomposed as

$$\hat{\rho}(t)=\mathrm{e}^{t\mathcal{L}}[\hat{\rho}(0)]=\hat{\rho}_{\rm ss}+\sum_{k\geqslant 2}c_k\mathrm{e}^{t\lambda_k}\hat{R}_k, \tag{23}$$

where λ_k are the Liouvillian eigenvalues, sorted for convenience as $0\geqslant \mathrm{Re}[\lambda_k]\geqslant \mathrm{Re}[\lambda_{k+1}]$, where we assume a single steady state $\hat{\rho}_{\rm ss}$ with eigenvalue $\lambda_1=0$ and $\hat{R}_k$ are the corresponding right eigenmatrices of the superoperator $\mathcal{L}$. The coefficients c_k depend on the initial state $\hat{\rho}(0)$ as $c_k=\mathrm{tr}[\hat{L}_k^\dagger\hat{\rho}(0)]$ where $\hat{L}_k$ are the left eigenmatrices normalized such that $\mathrm{tr}[\hat{L}_j^\dagger\hat{R}_k]=\delta_{jk}$.

In open quantum systems, metastability is typically observed as a consequence of a gap between two successive eigenvalues of the Liouvillian, say λ_n and λ_{n+1} (see figure 4). After $t>\tau_{n+1}$, all modes with $k>n+1$ give exponentially small contributions to the evolution and can be neglected. Here the system

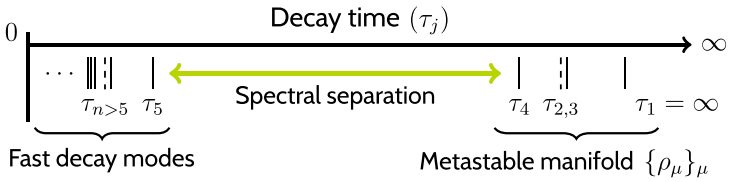

Figure 4. The spectrum of a Liouvillian superoperator with a metastable regime displays a large gap between two consecutive eigenvalues λ_k. Here we sketch the decay time $\tau_k^{-1} = -\mathrm{Re}[\lambda_k]$ of the eigenvalues. From left to right, we encounter the fast decaying modes with $\tau \ll 1$ separated by a large gap from the four modes defining the metastable manifold that includes the stable state corresponding to $\lambda_1 = 0$.

enters the metastable regime, where the evolution of a generic initial state $\hat{\rho}(0)$ can be decomposed as

$$\hat{\rho}(t) \approx \hat{\rho}_{\mathrm{ss}} + \sum_{k=2}^{n} c_k(t)\hat{R}_k = \mathcal{P}_{\mathrm{MM}}[\hat{\rho}(0)], \tag{24}$$

where $\mathcal{P}_{\mathrm{MM}}$ is a projector superoperator on the first n modes characterizing the metastable manifold. Such a manifold can induce a DFS or a noiseless subsystem structure [74], but we will focus here on the so-called *classical metastability*, where each state can be expressed as a convex combination of n disjoint metastable phases $\{\hat{\rho}_\mu\}$ [29],

$$\hat{\rho}(t) = \sum_{\mu=1}^{n} p_\mu(t)\hat{\rho}_\mu, \tag{25}$$

with $p_\mu(t) \geqslant 0$ the probability that the state is in the μth phase. The metastable phases correspond to physical states that do not evolve in time. Here we assume the possible corrections to classicality are negligible so that the metastable phases and derived quantities are well-defined within the framework of [29].

Then, the dynamics is fully encoded in the evolution of the probabilities $\{p_\mu(t)\}$, obtained from the set of projectors $\{\hat{P}_\mu\}$ defined as $\hat{P}_\mu = \sum_{k=1}^{n}(C^{-1})_{\mu k}\hat{L}_k$ with $(C)_{\mu k} = \mathrm{tr}\,\hat{L}_k^\dagger\hat{\rho}_\mu$. The projectors satisfy $\mathrm{tr}\,\hat{P}_\mu\hat{\rho}_\nu = \delta_{\mu\nu}$ and $\sum_\mu \hat{P}_\mu = \mathbb{I}$ but may have eigenvalues smaller than zero or exceeding one if the classicality corrections are large. Importantly, for a general quantum state $\hat{\sigma} \in \mathcal{B}(\mathcal{H})$, the value $p_\mu = \mathrm{tr}\,[\hat{P}_\mu\hat{\sigma}]$ represents the probability that the state $\hat{\sigma}$ evolves into the metastable phase $\hat{\rho}_\mu$ during the transient regime. Hence, this value is preserved until the final decay to the steady state for $t > \tau_n$. For this reason, the projectors can be used to define the basins of attraction of each pattern since any state with $p_\mu > 1/2$ is guaranteed by equation (25) to be found in the metastable phase $\hat{\rho}_\mu$ with the largest probability. In analogy to the steady state scenario (see section 6), the metastable phases $\hat{\rho}_\mu$ act as invariant states for the projective map $\mathcal{P}_{\mathrm{MM}}$ and the projectors $\hat{P}_\mu$ are the associated conserved quantities.

Therefore, any quantum system displaying classical metastable dynamics can be understood as an AM where (C1) the patterns are the disjoint metastable phases $\{\hat{\rho}_\mu\}$, invariant under the map $\mathcal{P}_{\mathrm{MM}}$; (C2) there exists a subspace

$$\mathcal{H}_\mu = \mathrm{span}\left\{|v_j^{(\mu)}\rangle \mid \hat{P}_\mu|v_j^{(\mu)}\rangle = \lambda_j^{(\mu)}|v_j^{(\mu)}\rangle, \lambda_j^{(\mu)} > \delta\right\}, \tag{26}$$

with $\delta \geqslant 1/2$ containing all the initial conditions evolving under the corresponding pattern with the highest probability, as well as the μth metastable phase; (C3) the subspaces $\mathcal{H}_\mu$ are approximately disjoint, and can be therefore regarded as basins of attraction. Here, 'approximately' is meant to remind that the classical metastability description is in general accurate up to some corrections, which are indeed responsible for dealing with the approximate orthogonal phases $\{\hat{\rho}_\mu\}$ and their approximate disjoint basins of attraction (26). Moreover, as discussed in [29], setting $\delta \geqslant 1/2$ permits one to deal with well-defined basins of attraction. Instead, generic eigenspaces $\mathcal{H}_\mu$ feature states decaying into non-trivial mixture of patterns, hence turning out to be non-disjoint.

The case of classical metastability falls into the category of QAM with orthogonal patterns, where the number of patterns depends on the dimension of the metastable manifold (the number of slow-decaying Liouvillian modes). Then, the appearance of a gap between the eigenvalues λ_n and λ_{n+1} allows one to store n patterns. The difference between the real parts of the eigenvalues determines the length of the metastable transient. The decay time to the metastable manifold is $\tau_{n+1} = -[\mathrm{Re}\lambda_{n+1}]^{-1}$, and $\tau_n = -[\mathrm{Re}\lambda_n]^{-1}$

determines the end of the metastable regime. Since the dynamics is frozen in between, a measurement can be taken at τ_{n+1} to determine the pattern. The longer we wait to measure, the more likely we are to get a wrong result since jumps between patterns occur at a rate of $1/\tau_n$. Of course, in the long time limit, all information is lost as the state decays to the final steady state.

Before proceeding further, we highlight the main differences between a QAM working in the steady state regime, as described by definition 1, and a QAM in the metastable scenario. First of all, it is worth noticing that, for metastable patterns, the association condition of equation (6) does not occur in the infinite time limit but in a transient regime $\tau_{n+1} < t < \tau_n$. Further, we also stress that while the basins of attraction of definition 1 are kept orthogonal, (both the supports of fixed points and decaying subspaces are orthogonal among each other), the ones defined by equation (26) are proven to be approximately disjoint, as commented above. One could attempt to similarly adopt a less strict requirement for the decomposition of the decaying subspace $\mathcal{D}$ of definition 1 into the decaying spaces $\mathcal{D}_\mu$. However, this would lead to a weaker definition of QAM. Indeed, at variance with the phenomenology of the classical metastability, there would be, *a priori*, no means to identify a parameter [similar to δ in equation (26)] allowing one to characterize and delimitate states evolving into non-trivial mixture of memories.

Finally, we note that the definition of storage capacity given in equation (19) is still valid. In this case, the number of patterns is determined by the number of metastable phases (the dimension of the metastable manifold $\mathcal{H}_{\mathrm{MM}}$) and the system size is still the total Hilbert space dimension

$$\alpha^{\mathrm{MM}} = \frac{\dim \mathcal{H}_{\mathrm{MM}}}{\dim \mathcal{H}}. \tag{27}$$

Again, in analogy with the steady state case, the metastable manifold represents the stable subspace of the system where memories are encoded and retrieved but the association happens in the full Hilbert space composed of both stable and decaying subspaces.

8. Examples

In this section, we will analyze three examples of QAM based on the theoretical framework constructed in previous sections.

8.1. Quantum random walk

An interesting approach to QAM was taken in [24], where the proposed system is a dissipative quantum walk that converges to the predefined patterns in the long time limit. Here, as in the classical HNN, the patterns $\{\boldsymbol{x}^\mu\}_{\mu=1}^{M_\perp}$ are represented by strings of n-bits, $\boldsymbol{x}^\mu = (x_1^\mu, x_2^\mu, \ldots, x_n^\mu)$ with $x_j^\mu \in \{0,1\}$, which are encoded in n two-dimensional quantum systems $\mathcal{H}_2$ such that $\boldsymbol{x}^\mu \to |x^\mu\rangle = |x_1^\mu\rangle|x_2^\mu\rangle\cdots|x_n^\mu\rangle$. Notice that, while the corresponding classical patterns are in general non-orthogonal, this (basis) encoding leads to orthogonal patterns, i.e. quantum states $\{|x^\mu\rangle\}$ satisfying $\langle x^\mu|x^\nu\rangle = \delta_{\mu\nu}$, so $M = M_\perp$. Thus, the stable subspace is spanned by the patterns, i.e. $\mathcal{S} = \mathrm{span}\{|x^\mu\rangle\}$, and any other state in $\mathcal{H}_2^{\otimes n}$ belongs to the decaying subspace.

The dynamics can be visualized as a dissipative quantum walk on an n-dimensional hypercube (see figure 5(a)), where the nodes are all possible vectors $\boldsymbol{\omega} = (\omega_1, \omega_2, \ldots, \omega_n) \in \{0,1\}^n$, and edges between two nodes exist if and only if their Hamming distance $d_{\mathrm{H}}(\boldsymbol{\omega}, \boldsymbol{\omega}') = \sum_{i=1}^n |\omega_i - \omega_i'|/2 = 1$, i.e. they differ only by one bit. Using this definition, we can identify the decaying subspace of the μth pattern as the collection of states that are closer to it in terms of Hamming distance than to any other pattern x^ν,

$$\mathcal{D}_\mu = \mathrm{span}\left\{|\omega\rangle \in \mathcal{S}^\perp \mid \arg\min_\nu d_{\mathrm{H}}(\boldsymbol{\omega}, \boldsymbol{x}^\nu) = \mu\right\}. \tag{28}$$

Then, the dissipative quantum walk must associate a state $|\omega\rangle \in \mathcal{D}_\mu$ with $|x^\mu\rangle$. This is engineered by ensuring that (C1) the patterns are invariant states of the Liouvillian superoperator, and (C2) the jump operators, denoted by $\hat{L}_{\omega\to\omega'}$, couple only states that reduce the Hamming distance towards a pattern,

$$\hat{L}_{\omega\to\omega'} = |\omega'\rangle\langle\omega| \text{ if } \min_\mu d_{\mathrm{H}}(\boldsymbol{\omega}', \boldsymbol{x}^\mu) < \min_\mu d_{\mathrm{H}}(\boldsymbol{\omega}, \boldsymbol{x}^\mu). \tag{29}$$

A jump between two states happens at a rate γ, so the walker needs a time $d_{\mathrm{H}}(\boldsymbol{\omega}, \boldsymbol{x}^\mu)/\gamma$ to reach the fixed point.

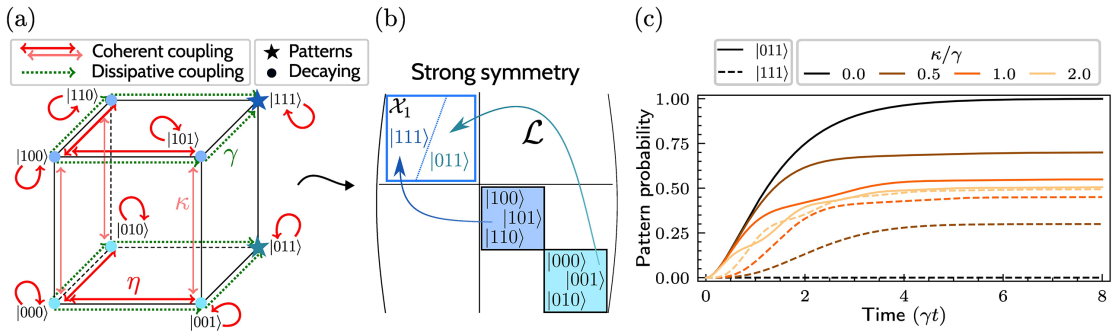

Figure 5. Dissipative quantum walk for QAM. (a) The nodes of the cube represent the possible states of the walker, and edges are connected between pairs of nodes if their Hamming distance is 1. The coherent dynamics couple states with a strength η if they belong to the same basin and κ otherwise. The dissipative part drives the states towards the corresponding fixed points with a rate γ. (b) Strong symmetry induced in the Liouvillian compatible with figure 3 for $\kappa = 0$. (c) Exact evolution of the initial state $|000\rangle$ for different coupling values between the basins and fixed $\eta/\gamma = 0.1$. The y-axis shows the overlap of the evolving state with the patterns: $|011\rangle$ (solid lines) and $|111\rangle$ (dashed lines). The association to the pattern $|011\rangle$ is perfect only for vanishing κ (black lines). For $\kappa > 0$ the symmetry is lost, and the probability of retrieving the second pattern increases until $\kappa > \gamma$ where both patterns become equally probable.

The dynamics is completed by a Hamiltonian that couples all nodes at distance 1 except the patterns [24]. Hence, the Hamiltonian matrix reads

$$\langle\omega'|\hat{H}|\omega\rangle = \begin{cases} \eta & |\omega\rangle, |\omega'\rangle \in \mathcal{D}_\mu \\ \kappa & |\omega\rangle \in \mathcal{D}_\mu \text{and } |\omega'\rangle \in \mathcal{D}_\nu \ \mu \neq \nu \end{cases}, \tag{30}$$

where nodes are coherently coupled with strength η to themselves and to any other node in the same basin, and with strength κ to nodes in different basins. The complete Liouvillian is thus $\mathcal{L}(\hat{\rho}) = -\mathrm{i}[\hat{H}, \hat{\rho}]$ $+\sum_{\omega,\omega'} \gamma \mathcal{D}[\hat{L}_{\omega\to\omega'}]\hat{\rho}$, where $\mathcal{D}[\hat{O}]\hat{\rho} = \hat{O}\hat{\rho}\hat{O}^\dagger - \frac{1}{2}\{\hat{O}^\dagger\hat{O}, \hat{\rho}\}$. The patterns are steady states by construction, and in fact, the stable subspace is a DFS where the coherences between patterns are also preserved $(\mathcal{L}(|x^\mu\rangle\langle x^\nu|) = 0)$.

For instance, in the example of figure 5, there are two patterns $\boldsymbol{x}^1 = (0,1,1)$ and $\boldsymbol{x}^2 = (1,1,1)$ with associated decaying subspaces $\mathcal{D}_1 = \text{span}\{|000\rangle, |001\rangle, |010\rangle\}$ and $\mathcal{D}_2 = \text{span}\{|100\rangle, |101\rangle, |110\rangle\}$ respectively. The collection of jump operators produces bit-flips in the last two qubits to drive the walker towards the patterns, while the coherent Hamiltonian produces oscillations between (κ) and within (η) the basins.

Let us first focus on the case $\kappa = 0$. In panel (a) we can see that the cube separates into two disconnected regions containing the states in $\mathcal{H}_1$ (bottom face) and $\mathcal{H}_2$ (top face). Moreover, we can observe the presence of a strong symmetry $\hat{P} = \hat{\sigma}_z \otimes \mathbb{I}_2 \otimes \mathbb{I}_2$, which means that the overlap with the first qubit is preserved during the evolution. That is, for any initial state $\hat{\sigma} \in \mathcal{B}(\mathcal{H})$ it holds that $\text{tr}[\hat{P}\hat{\sigma}(t=0)] = \text{tr}[\hat{P}\hat{\sigma}(t=\infty)]$, such that if $\hat{\sigma} \in \mathcal{B}(\mathcal{H}_\mu)$ then $\lim_{t\to\infty} \mathrm{e}^{\mathcal{L}t}(\hat{\sigma}) = |x^\mu\rangle\langle x^\mu|$, thus satisfying the associativity condition (6). The AM implemented by a quantum random walk with strong symmetry associates a pure state $|\boldsymbol{s}\rangle$ with $\boldsymbol{s} \in \{0,1\}^n$ to the closest pattern $\{\boldsymbol{x}^\mu\}$ in terms of its Hamming distance.

If the coupling between the basins is $\kappa > 0$, then the strong symmetry is broken, and information can flow between them. As an example, in panel (c) we show the time evolution of the observables $\hat{P}_{011} = |011\rangle\langle 011|$ and $\hat{P}_{111} = |111\rangle\langle 111|$ for the initial state $|000\rangle$. Increasing the value of the coupling κ decreases the final retrieval probability since the walker has a non-vanishing probability of going to the other basin. This corresponds to a regime where condition C3 is no longer satisfied as the decaying subspaces are mixed. Only the case $\kappa = 0$ leads to perfect retrieval, as expected from the symmetry. Conversely, when the coherent coupling is larger than the dissipation rate $(\kappa/\gamma > 1)$, the walker ends up in an equal mixture of both patterns. Therefore, this system is a valid AM only in the regime $\kappa/\gamma \sim 0$.

Furthermore, we can calculate the maximum storage capacity of this system. By construction, the model can only store classical-like patterns that are orthogonal. Then, as shown in section 4.1, the maximum storage capacity is $1/2$. This limit corresponds to storing half of the bit-strings (2^{n-1}) as patterns, while the other half belongs to the decaying subspace. For example, we can choose as patterns all the states satisfying $|x^\mu\rangle = [\otimes_{i=1}^{n-1}|x_i^\mu\rangle]|0\rangle$ (even states), and we can associate them with the odd state $|\omega^\mu\rangle = X_n|x^\mu\rangle$ $= [\otimes_{i=1}^{n-1}|x_i^\mu\rangle]|1\rangle$.

This example proves the validity of our formulation to explain previous models that use symmetry to realize a QAM. This particular model allows the perfect association of classical bit strings and may therefore be useful for tasks involving classical data. This system has been experimentally realized using photonic chips [25], but other platforms, such as ensembles of qubits, may also be useful. In fact, it is possible to understand this model as an n-spin ensemble, where for the particular example in figure 5(a) the Liouvillian reads $\mathcal{L}(\hat{\rho}) = \sum_j [-\mathrm{i}\frac{\omega}{2}\hat{\sigma}_j^z + \kappa'\hat{\sigma}_j^x, \hat{\rho}] + \gamma D[\hat{\sigma}_2^-]\hat{\rho} + \gamma D[\hat{\sigma}_3^-]\hat{\rho}$ where $\hat{\sigma}_j^- = |1\rangle\langle 0|$ is the decay operator on the jth qubit and $\hat{\sigma}_j^{x,z}$ are the Pauli matrices. This produces the same dynamics as the dissipative quantum walk and has the patterns as steady states when $\kappa' = 0$ (in fact, it is the example of the amplitude decaying channel on the last two qubits).

The dissipative quantum random walk for QAM can be applied as a quantum error correction protocol for bit-flip errors. For example, let us consider the three-qubit code, where one has the logical states $|0_L\rangle = |000\rangle$ and $|1_L\rangle = |111\rangle$ [39]. Here, single-bit flip errors can be typically corrected by a majority voting mechanism. In the language of AM, this means that states that differ by a single bit from one of the two logical states are associated with that bit. Hence, the dissipative quantum walk can be considered as an autonomous quantum error correction for bit-flip errors. Indeed, symmetry protects the system from bit flips by associating errors within the error space with the corrected state. Moreover, since the stable subspace of the system is a DFS, quantum coherences are preserved and it allows the storage of a qubit.

8.2. Driven-dissipative resonator

Driven-dissipative resonators are well-studied systems displaying rich dynamical phenomena like metastability and dissipative phase transitions [75] and have been recently employed for quantum memories [76]. In particular, these oscillators have been shown useful for QAM in a metastable regime leading to improved storage capacities [26] and allowing the storage of genuine quantum states [27]. In this section, we will review the most important characteristics of the metastable QAM and show the possibility of having permanent memories. Thus highlighting the versatility of these systems for storing different types of quantum patterns.

The oscillator is described by a GKSL equation

$$\frac{\partial\hat{\rho}}{\partial t} = -\mathrm{i}\left[\hat{H}_n, \hat{\rho}\right] + \gamma_1\mathcal{D}\left[\hat{a}\right]\hat{\rho} + \gamma_n\mathcal{D}\left[\hat{a}^n\right]\hat{\rho}, \tag{31}$$

where we have standard terms for linear (single-photon) and nonlinear (multiphoton) damping [77, 78] with rates γ_1 and γ_n respectively. The Hamiltonian, which contains a n-order squeezing drive [75, 79, 80], in the rotation frame and after the parametric approximation is

$$\hat{H}_n = \Delta\hat{a}^\dagger\hat{a} + \mathrm{i}\eta\left[\hat{a}^n\mathrm{e}^{\mathrm{i}\theta_0 n} - \left(\hat{a}^\dagger\right)^n\mathrm{e}^{-\mathrm{i}\theta_0 n}\right]. \tag{32}$$

Here, $\Delta = \omega_0 - \omega_s$ is the detuning between the natural oscillator frequency and that of the squeezing force, η, and θ_0 the magnitude and phase of the driving, respectively. We observe that the model possesses $\mathbb{Z}_n$ symmetry, that is, the transformation $\hat{a} \to \hat{a}\exp(\mathrm{i}2\pi/n)$ leaves the master equation invariant [75]. The interplay between driving and dissipation, together with the rotation symmetry of the system, leads to the generation of n symmetrically distributed coherent states $\{|\alpha_j\rangle\}_{j=1}^n$ in the steady state, where $\alpha_j = r\exp(\mathrm{i}\theta_j)$ with $r^n = 2\eta/\gamma$ and $\theta_j = 2\pi j/n + \theta_0$.

In the following parts, we will study the use of the driven-dissipative oscillator for QAM in two regimes: the weak symmetry one, where the coherent states are metastable, and the strong symmetry one, where the coherent states form n-cat states that are steady states of the dynamics. This allows us to illustrate metastable and stable patterns encoding for QAM, in terms of coherent states and cat states, respectively.

8.2.1. Metastable encoding

In the presence of linear dissipation ($\gamma_1 > 0$), the oscillator has a metastable phase that separates the slowest decaying n Liouvillian modes (including the steady state) from the rest. These n modes define n metastable phases $\{\hat{\rho}_\mu\}_{\mu=1}^n$ corresponding to the n lobes forming the steady state, so $\hat{\rho}_\mu = |\alpha_\mu\rangle\langle\alpha_\mu|$. In the upper left part of figure 6 we see an example for $n = 3$, where three symmetrically distributed coherent states define the quantum patterns.

We can also identify a basin of attraction that divides the phase space into n regions. The projector on each of these basins can be written as

$$\hat{P}_\mu = \frac{1}{\pi}\int_{\theta_j-\pi/n}^{\theta_j+\pi/n}\mathrm{d}\varphi\int_0^\infty \mathrm{d}R\, R|R\mathrm{e}^{\mathrm{i}\varphi}\rangle\langle R\mathrm{e}^{\mathrm{i}\varphi}|\ , \tag{33}$$

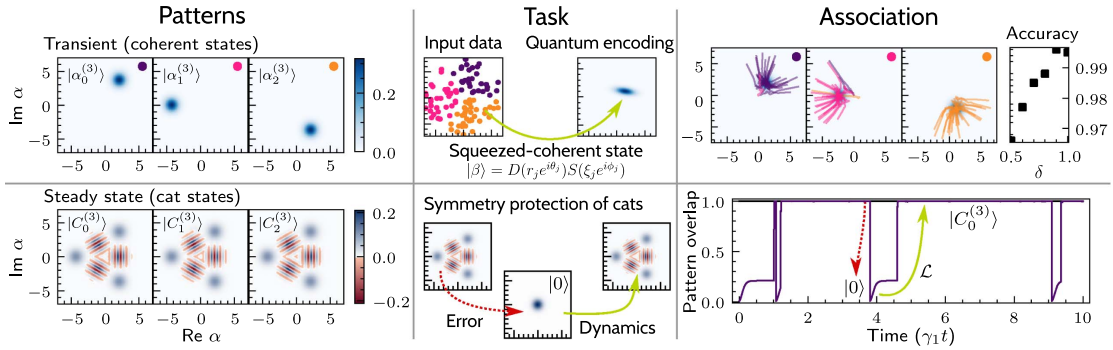

Figure 6. Driven-dissipative resonator for QAM. Parameters: $n = m = 3$, $\gamma_3 = 0.2$, $\eta = 1.56$, $\Delta = 0.4$ and $\theta_0 = 0$. Upper: weak symmetry regime ($\gamma_1 = 1$). (left) Patterns are defined by the metastable phases: n symmetrically distributed coherent states. (center) Initial data points are encoded in quantum states such as squeezed states, each of which should be associated with the nearest pattern identified by the color (violet $\to \alpha_0$, magenta $\to \alpha_1$ and orange $\to \alpha_2$). The basins of attraction (equation (26)) that identify the correct pattern are defined with $\delta = 0.5$. (right) The evolution of the state drives the system towards one of the patterns as soon as the system enters the metastable transient. We see the result of the classification of 100 states, where each line is a single trajectory for each initial state in the left part. The upper-right colored dots represent the lobe that the state should be associated with while the trajectory color indicates the measured lobe after association. An accuracy of 0.96 is obtained for $\delta = 0.5$ but increasing the spacing between basins leads to higher accuracy as expected. Lower: strong symmetry regime ($\gamma_1 = 0$). (Left) Patterns are defined by the steady states of the system: n-cat states. (center) The task of the QAM is to correct amplitude damping errors which bring the system to the empty state $|0\rangle$. (right) Strong symmetry preserves the parity of the original states, so the states converge to the cat state of the corresponding parity.

so that all coherent states whose phase is in the interval $[\theta_j - \pi/n, \theta_j + \pi/n]$ will be classified as being in the jth basin. Then, the subspaces given by equation (26), with the projectors defined by equation (33), identify the basins of attraction for each pattern. However, since coherent states form an overcomplete basis, these are disjoint but only approximately orthogonal, as states lying close to the boundary between two basins have a similar probability of converging to both lobes. To prevent this, we may choose a larger value of δ that would correspond to less distorted patterns.

In figure 6, an oscillator with $n = m = 3$ is used to restore coherent states. The initial states can be obtained from classical data encoded in squeezed coherent states, or directly from quantum inputs. For example, discrete modulated continuous-variable quantum key distribution protocols use symmetric distributed coherent states to encode the keys [81, 82]. The states typically suffer from noise during transmission, which distorts the states. The task is to use QAM to recover the original states, characterized by the colors of the points in the middle panel. For example, the initial points are randomly chosen coherent states satisfying that the overlap with a basin is at least $\delta = 0.7$ (see equation (26)).

For the reconstruction task, we inject 100 coherent states and compute a single trajectory for each of them. At the start of the metastable transient an unambiguous measurement is performed as explained in [26]. The state is associated with a lobe if the measurement triggers the corresponding projector $\Pi_\mu = |\alpha_\mu\rangle\langle\alpha_\mu|$ [83]. The trajectory for each lobe is shown in the left panel of figure 6. States correctly classified match the color of the trajectory with the plot. In this example, all states are classified, and 96% of them are reconstructed correctly. The errors are produced by random jumps between lobes and between a lobe and the steady state. The longer we wait to measure inside the metastable regime, the more likely is that a jump will occur. Increasing the value of $\delta \geqslant 0.8$ leads to a perfect retrieval accuracy, as the basins are more orthogonal, although already with $\delta = 1/2$ we can achieve accuracies above 95%.

8.2.2. Cat state encoding

When the linear dissipation is turned off ($\gamma_1 = 0$), the system displays a strong $\mathbb{Z}_n$ symmetry which divides the Hilbert space into n symmetry sectors. In each sector there exists a steady state $\hat{\rho}_\mu$ ($\mu = 1, \ldots, n$) and we can identify n conserved quantities $\{\hat{P}_\mu\}$ such that $\mathrm{tr} P_\nu \hat{\rho}_\mu = \delta_{\mu\nu}$. These states for a driven-dissipative nonlinear oscillator correspond to multimode n-cat states

$$\left|C_\mu^{(n)}\right\rangle = \frac{1}{\sqrt{n}} \sum_{k=0}^{n-1} \mathrm{e}^{\mathrm{i}2\pi\mu k/n} |\alpha_k\rangle \quad j = 0, \ldots, n-1, \tag{34}$$

where the coherent states $|\alpha_k\rangle$ are the same as in the previous case. For $n = 2$, this reduces to the even and odd cat states $|C_\pm^{(2)}\rangle = (|+\alpha\rangle \pm |-\alpha\rangle)/\sqrt{2}$, and the conserved quantities are the projectors onto the even and odd parity sectors, respectively. In general, the μth cat state contains only Fock states, $|na + \mu\rangle$ where $a \in \mathbb{N}$, and the conserved quantities can be expressed as $\hat{P}_\mu = \sum_a |na + \mu\rangle\langle na + \mu|$. Treating each cat state as

a pattern, the strong symmetry enables a QAM since any state belonging to a symmetry sector will be associated with the corresponding cat state. Even though the Hilbert space is infinite-dimensional, we can also define a stable and a decaying subspace. The stable subspace, depending on the system parameters [75, 84], is spanned either only by the cat states, forming n irreducible subspaces $\{\mathcal{S}_\mu\}_{\mu=0}^{n-1}$, or also by their coherences $|C_\mu^{(n)}\rangle\langle C_\nu^{(n)}|$, forming a three-dimensional DFS $\mathcal{X}$. The latter would allow the storage not only of the multimode cat states but also of any linear superposition of lobes such as a cat state between two lobes, i.e. $|\alpha_0\rangle \pm |\alpha_1\rangle$. By exploiting the strong symmetry of the model, the eigenspaces of the conserved quantities, that we called $\hat{P}_\mu$, identify the basin of attractions $\mathcal{H}_\mu$ for each cat state, and the associated decaying space is the orthogonal complement to $\mathcal{S}_\mu$ with respect to $\mathcal{H}_\mu$.

This situation resembles the example of the dissipative random walk, where the block structure of the Liouvillian generated by a strong symmetry allows for perfect association between decaying and stable states. An example is shown in the lower part of figure 6 for $n = m = 3$. There are three cat states with parity eigenvalue 0, $2\pi/3$, and $-2\pi/3$ that can be used as patterns. Such multicomponent cat states have been experimentally realized in superconducting platforms [85] with applications to quantum error correction [86].

In the lower part of figure 6 we perform a particular QAM task where the patterns are the three-mode cat states (equation (34) with $n = 3$). Here, the state may undergo an amplitude damping channel where, with some probability, the state is reset to the ground state $|0\rangle$. Then, the QAM restores the state. Indeed, since the state is symmetry-protected, the cat state is recovered after a short time, due to its dynamics. An example of such a trajectory is seen in the bottom right panel of figure 6, where we plot the overlap with the cat state $|C_0^{(3)}\rangle$. As soon as the error occurs, the state is associated back to the cat state.

Note that, measuring the parity of the state is not enough to determine if the evolution has converged to the pattern. Indeed, in this example, parity is always conserved but the state jumps from the vacuum state to the cat state. Hence, in general, the symmetry guarantees that a state will be associated with the steady state with the same symmetry, but we cannot use the respective conserved quantity to determine if the association has happened or not. For that, we must resolve to an operator that can identify if the state has evolved into the pattern or not.

8.3. Geometrically uniform states

In this section, we extend the example introduced in section 5.2 to model an AM that stores many non-orthogonal patterns in a two-dimensional DFS. Consider a system of n qubits where the total Hilbert space is $\mathcal{H} = \mathcal{H}_2^{\otimes n}$ spanned by the states $\{|x\rangle = |x_1\rangle|x_2\rangle\cdots|x_n\rangle\}_{x=0}^{2^n-1}$ where we denote the elements of such a basis as $x = \sum_{t=1}^{n} x_t 2^{n-t}$, and the term $|x_t\rangle$ with $x_t \in \{0, 1\}$ represents the tth qubit basis and $t = 1, \ldots, n$. We want to construct a two-dimensional stable subspace that allows us to store the GUS. For this, we arbitrarily chose two states: $|\tilde{0}\rangle = |0\rangle^{\otimes n}$ and $|\tilde{1}\rangle = |1\rangle^{\otimes n}$. The patterns stored in $\mathcal{S}$ correspond to a number $M_{\not\perp} \equiv M > 2$ of GUS, $|\psi_\ell\rangle = \hat{U}^{\ell-1}|\psi\rangle$, $\ell = 1, \ldots, M$, where $\hat{U}$ is a unitary operator, $\hat{U} = \exp(-\mathrm{i}2\pi\,\hat{\sigma}_y/M)$, so that $\hat{U}^M = \mathbb{I}_2$ and $\hat{\sigma}_y = \mathrm{i}(|\tilde{1}\rangle\langle\tilde{0}| - |\tilde{0}\rangle\langle\tilde{1}|)$. Then the stable subspace consists of only one DFS $\mathcal{S} = \mathcal{X}_1$ (with respect to the notation introduced in section 4.2, $M_\perp = 0$ and $C_{\not\perp} = 1$) [87].

As explained in section 4.2, for each pattern there must exist a decaying subspace consisting of all states associated with the particular pattern. Since there is only one DFS in the stable subspace, we can decompose the decaying subset as $\mathcal{D} = \bigoplus_{\ell=1}^{M} \mathcal{D}_\ell$, where we have omitted the index $\tau = 1$, which appears in equation (14), for the sake of easier notation. From the definition of the stable subspace follows that a basis of the complete decaying part can be obtained as $\mathcal{D} = \mathcal{S}^\perp = \mathrm{span}\{|\omega_x\rangle\}_{x=1}^{2^n-2}$, with dimension $2^n - 2$. We thus define the ℓth decaying subspace according to

$$\mathcal{D}_\ell = \mathrm{span}\{|\omega_x\rangle \in \mathcal{D} \mid x \mod M = \ell\}, \tag{35}$$

so that the decaying states $|\omega_x\rangle$ are associated with the ℓth rotated pattern if the label x modulus M is exactly ℓ. As an example, if we consider a total system made of $n = 3$ qubits where we store $M = 3$ patterns in the DFS spanned by $\{|0\rangle, |7\rangle\}$, the three decaying subspaces are $\mathcal{D}_1 = \mathrm{span}\{|1\rangle, |4\rangle\}$, $\mathcal{D}_2 = \mathrm{span}\{|2\rangle, |5\rangle\}$ and $\mathcal{D}_3 = \mathrm{span}\{|3\rangle, |6\rangle\}$. Likewise, when considering $M = 4$ patterns, we will build the following four decaying subspaces, $\mathcal{D}_1 = \mathrm{span}\{|1\rangle, |5\rangle\}$, $\mathcal{D}_2 = \mathrm{span}\{|2\rangle, |6\rangle\}$, $\mathcal{D}_3 = \mathrm{span}\{|3\rangle\}$, and $\mathcal{D}_4 = \mathrm{span}\{|4\rangle\}$. Note that, in the generic case, this construction leads to decaying subspaces $\mathcal{D}_\ell$ not all sharing the same dimensions, as shown in figure 7.

The expression for the Kraus operators follows the one given in equation (15)–(17), where the part acting on the stable subspace is proportional to the identity, the part acting on the ℓth decaying subspace reads

$$K_{\alpha,\ell}^{\mathrm{D}} \equiv K_{\alpha,1,\ell}^{\mathrm{D}} = \sum_{x=0}^{d_\ell - 1} c_{\ell,x}^{\alpha} |\omega_{xM+\ell}^{\ell}\rangle\langle\omega_{xM+\ell}^{\ell}|, \tag{36}$$

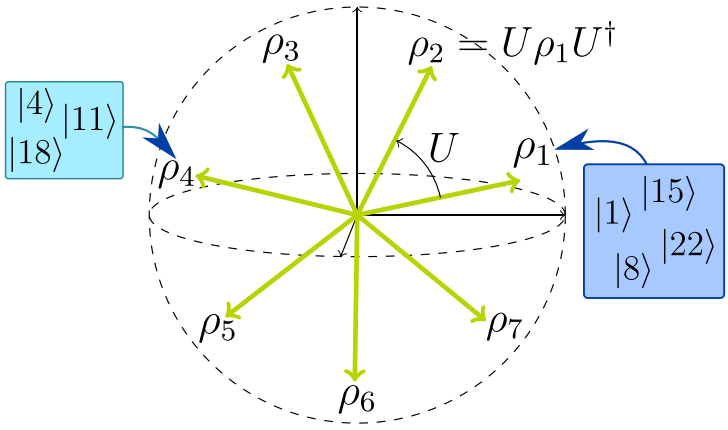

Figure 7. Bloch-sphere representation of the stable subspace characterized by a two-dimensional DFS in which seven GUS defined by the unitary $\hat{U}$ are stored. For each pattern $\hat{\rho}_\mu$, there is a decaying subspace formed by states in $\mathcal{H}_2^{\otimes n}$ whose decimal representation module M is equal to μ.

for $\ell = 1, \ldots, M$ with $d_\ell = \lfloor (N^D - \ell - 1)/M \rfloor + 1$. And finally, the part mixing stable and decaying is

$$K_\alpha^{\mathrm{SD}} \equiv K_{\alpha,1}^{\mathrm{SD}} = \sum_{\ell=1}^{M} \sum_{j=0}^{1} \sum_{x=0}^{d_\ell - 1} b_{\ell,j,x}^{\alpha} |\tilde{j}\rangle\langle\omega_{xM+\ell}^{\ell}|. \tag{37}$$

Reminding that we aim at storing GUS as patterns, i.e. the states

$$|\psi_\ell\rangle = \hat{U}^{\ell-1}|\psi\rangle = \sum_{j=0}^{1} \psi_j \mathrm{e}^{-\mathrm{i}\pi j\ell/M} |\tilde{j}\rangle, \tag{38}$$

the associativity condition as formulated in equation (C5) reads

$$\sum_\alpha \left(b_{\ell,k,y}^{\alpha}\right)^* b_{\ell',j,x}^{\alpha} = \delta_{\ell\ell'} \kappa_{xy}^{\ell} \langle\tilde{j}|\hat{U}^{\ell-1}|\psi\rangle\langle\psi|(\hat{U}^{\ell'-1})^\dagger|\tilde{k}\rangle, \tag{39}$$

which can be expressed as

$$\sum_\alpha (b_{\ell,k,y}^{\alpha})^* b_{\ell,j,x}^{\alpha} = \kappa_{xy}^{\ell} \psi_j \psi_k^* \mathrm{e}^{-\mathrm{i}\pi\ell(j-k)/M}. \tag{40}$$

By employing the results in appendix C.2, the parameters κ_{xy}^{ℓ}, can be further written as $\kappa_{xy}^{\ell} = \delta_{xy}(\kappa_x^{\ell})^2$, where κ_x^{ℓ} is given in terms of the decaying parameters $c_{\ell,x}^{\alpha}$ as in equation (C7). As such, the mixing parameters $b_{\ell,j,x}^{\alpha}$ need to satisfy

$$\sum_\alpha \left(b_{\ell,k,x}^{\alpha}\right)^* b_{\ell,j,x}^{\alpha} = \left(\kappa_x^{\ell}\right)^2 \psi_j \psi_k^* \mathrm{e}^{-\mathrm{i}\pi\ell(j-k)/M}. \tag{41}$$

Then, a simple solution of the above equation can be derived by associating a single Kraus operator to each collection of non-vanishing mixing terms, $\{b_{\ell,j,x}, \forall j\}$, which is uniquely identified by the pair (ℓ, x). In this case, the mixing parameters need to satisfy

$$b_{\ell,j,x}^{\alpha} = \psi_j \kappa_x^{\ell} \exp\left(\mathrm{i}\frac{2\pi}{M} j\ell\right) \delta_{\alpha-2,xM+\ell}. \tag{42}$$

First of all, notice that the CPTP condition in equation (C6) is automatically satisfied with this choice. Secondly, we further took into account that there are two Kraus operators acting only on the stable subspace as $\hat{K}_\alpha^{\mathrm{S}} = a_\alpha \mathbb{I}_{\mathrm{S}}$ for $\alpha = 1, 2$ (and $K_\alpha^{\mathrm{S}} = 0$ for $\alpha > 2$) (see equation (11*b*)). Hence, the final form of the map is

$$\hat{K}_1 = [a_1 \mathbb{I}_{\mathrm{S}}] \oplus \left[\sum_{\ell=1}^{M} \sum_{x=0}^{d_\ell - 1} \sqrt{1 - |\kappa_x^{\ell}|^2} |\omega_{xM+\ell}\rangle\langle\omega_{xM+\ell}|\right], \tag{43a}$$

$$\hat{K}_2 = [a_2 \mathbb{I}_{\mathrm{S}}] \oplus \mathbb{0}, \tag{43b}$$

$$\hat{K}_\alpha = \sum_{j=0}^{1} \psi_j \kappa_x^\ell \exp\left[\mathrm{i}\frac{2\pi j}{M}\ell\right] |j\rangle\langle\omega_{xM+\ell}|\delta_{\alpha-2,xM+\ell}, \quad \alpha = 3,\ldots,2^n+2. \tag{43c}$$

The previous map performs perfect association between the decaying states in each basin ($\mathcal{D}_\ell$) and the corresponding pattern ($|\psi_\ell\rangle$).

Now, we can calculate the storage capacity of the model using equation (20). Here, the dimension of the stable subspace is $N^{\mathrm{S}} = 2$, and the dimension of the decaying subspace is $N^{\mathrm{D}} = 2^n - 2$. Then,

$$\alpha^{\mathrm{Q}} = \frac{M}{2+2^n-2} = \frac{M}{2^n}, \tag{44}$$

where we note that M is only bounded by N^{D}, as there must be at least a decaying state for each pattern. Thus, in the limit $M \to 2^n - 2$ we arrive at $\alpha^{\mathrm{Q}} \to \alpha_c^{\mathrm{Q}} \approx 1$.

However, the classical storage capacity is smaller because we have to retrieve the information, that is, we need to discriminate the patterns. The optimal measurement strategy to maximize the success probability of discriminating GUS is the square-root measurement $P_{\mathrm{succ}} = |\langle\psi|\hat{\Phi}^{-1/2}|\psi\rangle|^2$, where $\hat{\Phi} = \sum_k |\psi_k\rangle\langle\psi_k|$ [71]. For GUS, we have $\hat{\Phi} = (M/N^{\mathrm{S}})\mathbb{I}_{\mathrm{S}}$ so $\hat{\Phi}^{-1/2} = \sqrt{N^{\mathrm{S}}/M}\mathbb{I}_{\mathrm{S}}$. and $P_{\mathrm{succ}} = N^{\mathrm{S}}/M$. Then, the classical storage capacity is

$$\alpha_c^{\mathrm{QC}} = \frac{N^{\mathrm{S}}}{M}\frac{M}{N^{\mathrm{S}}+N^{\mathrm{D}}} = \frac{N^{\mathrm{S}}}{N^{\mathrm{S}}+N^{\mathrm{D}}} = \frac{2}{2^n}, \tag{45}$$

which is the storage capacity one gets when storing two orthogonal patterns in a two-dimensional stable subspace. In other words, due to the measurement, the maximum storage capacity is limited by the storage capacity of orthogonal patterns. But, of course, this storage capacity is much smaller than α_c^{Q} in equation (44).

9. Discussion

The general framework for QAM elucidates their key features, underlying principles, and limitations. This unified approach also facilitates meaningful comparisons among diverse recent models. Initially, QAM was framed as a modified version of Grover's search algorithm [7]. This formulation can be regarded as a pattern completion problem rather than an association between the initial state and the target [13]. Patterns are encoded as classical bit strings in n qubits, and the algorithm searches the space of all possible patterns for those that are identical in the first $n-x$ qubits to the input. However, the algorithm is not able to restore imperfect preparation, differing therefore from a QAM. Moreover, because of its unitary nature, this approach departs from the original Hopfield formulation, as the patterns in question are not fixed points of the dynamics [7, 13]. Indeed, Grover's algorithm requires an optimal number of iterations depending on the starting point and the number of patterns. A possible solution is to use the modified Grover search method where the target states are fixed points [88–90]. Interestingly, even though some versions of this algorithm may store an exponential number of classical patterns [7, 8, 91, 92], it also introduces an exponential number of spurious memories. This is because any state in the Hilbert space has a non-zero probability of retrieval (decreasing with the dimension of the Hilbert space) so any state that is not a pattern is a spurious memory.

More in general, unitary-based QAM cannot exhibit fixed points of the dynamics, with the exception of the trivial (identity) case. Hence, these unitary approaches need to estimate beforehand the optimal number of applications of the unitary gate (or the optimal time to evolve a Hamiltonian) to retrieve the desired pattern with the highest probability. For instance, [8] reports that 80 repetitions of the algorithm are needed to retrieve the pattern with probability $1.4 \cdot 10^{-4}$. Similarly, the proposals of [10, 11] use a repeat-until-success strategy that measures the correct pattern depending on the Hamming distance between the input and all the patterns. As for the capacity of these proposals, it is limited by that of the employed Hebbian learning rule.

Complementary to the quantum circuit-based proposals discussed above, open quantum system approaches (analog) have been recently proposed and analyzed [17, 19–21, 59]. These contributions investigate the conditions under which some quantum many-body spin systems can effectively show AM behavior through the use of engineered dissipation. In contrast with unitary proposals, this allows the system to exhibit multiple fixed points, which play the roles of patterns. Notably, they make use of the Hebbian's prescription to embed target spin configurations, i.e. the memories, and therefore the latter can be regarded as classical ones. Within the framework outlined in section 3, the quantum map modeling these types of generalizations describes Markovian dynamics, $\Lambda(\bullet) = \mathrm{e}^{\mathcal{L}t}(\bullet)$. The evolution governed by the latter is analyzed in these works in specific limiting regimes (e.g. the thermodynamic limit [17, 19], or some

perturbative regime concerning terms of the dynamical generator [21]) at present. Here, the resulting effective evolution enables the system to operate as an AM. Within our framework, this can be understood as follows: condition C1, which requires multiple fixed points for the map, is satisfied by employing the Hebbian prescription, which sets classical patterns as fixed points of the effective evolution. Further, the dynamical equations emerging from the latter describe time-dependent variables (rather than operators), i.e. loosely speaking, some classical evolution (see [93] for a rigorous treatment). Such a dynamical system displays finite basins of attraction for each pattern, consistently with condition C2. While these QAM models in many-body systems are limited to classical regimes, our framework provides a foundation for exploring the quantum regime, presenting a promising avenue for future research.

Looking at further proposals in the existing literature, we identify some models of QAM that can perform effective association, albeit storing patterns only probabilistically [8, 10] while other models accomplish perfect storing of patterns in terms fixed points, yet lacking the association property [28]. Classically, the two features of stability and association go hand in hand, as can be seen, for example, in the HNN. Here, the non-linear dynamics, equipped with the Hebbian learning rule, guarantees that patterns are stable states with non-vanishing basins of attraction, at least below the critical storage capacity. To define a functioning QAM, however, the stability of patterns and the association between similar states must be individually addressed. In section 3, we have established the conditions under which we can achieve both features via CPTP maps.

The two main ingredients in the process of association identified in the discussed framework are dissipation and symmetry. Regarding dissipation, engineered losses act as a mechanism to drive the state of the system into a small subset of long-lived states. This aspect is common to quantum machine learning algorithms such as quantum reservoir computing [94, 95], quantum neural networks [53, 96] or variational quantum algorithms [97, 98], but also in algorithms such as state preparation [99, 100], and quantum error correction [101, 102]. This suggests the usefulness of our framework beyond QAM. Engineered dissipation can be implemented both in quantum circuits using the collision model algorithm [103], as experimentally demonstrated on the IBM platform [104], and in analog devices using the techniques introduced in [105].

Moving forward to the role of symmetries, they allow perfect discrimination between states that fall in the same symmetry sector. Previous research has shown that quantum machine learning models with the same symmetry as the data can avoid training problems and alleviate barren plateaus [106–108]. QAM also takes advantage of symmetries in quantum systems to perform the association process, allowing the storage of stable patterns in open quantum systems featuring strong symmetry or metastable patterns in the case of weak symmetry. For example, in section 8.1 we show the implementation of autonomous quantum error correction protocols [76, 101] where the patterns are fixed points of the dynamics and the error space is corrected dynamically thanks to a strong symmetry by associating the erroneous states with the correct logical qubits [73]. In another example proposed in section 8.2, we show that the metastable phase in a driven-dissipative resonator can be used to correct states generated by discrete-modulated continuous-variable quantum key distribution protocols, both of which share the same discrete rotational symmetry. The developed QAM framework sets therefore the basis for a broader context of applications, such as quantum memories or error correction, and also contributes to establishing the interplay between dissipation and symmetry in quantum machine learning.

We emphasize that the generality of the proposed formulation allows the storage of arbitrary quantum states as patterns, going beyond the classical-like patterns typically employed in previous formulations of QAM [7, 10, 17]. Indeed, the proposed general map can target all possible states, as, for instance, the case of cat states discussed in section 8.2. By exploiting the general properties of quantum channels, we have constructed maps that are not constrained by the limitations of the classical Hebbian rule. In our case, the storage of quantum patterns is permitted by the learning rule introduced in equation (12), which ultimately allows us to deal with quantum data [6] and to potentially store an exponentially large number of patterns efficiently.

Moreover, in section 5, we have proposed a simple, yet universal, definition of the quantum storage capacity that conveys the classical idea of quantifying the density of faithfully stored information in a system. Using this definition, we have separately established its bounds in the case of quantum outputs and also in the case of classical outputs, where the effect of measurements was considered. Interestingly, allowing for non-orthogonal patterns can enable an increase of the critical storage capacity for quantum outputs, even though in the case of classical patterns (after measurement), one encounters similar limitations in the association (success) probability, as in classical AM when correlated patterns are allowed.

The comparison with classical AM models is also interesting but not straightforward as patterns in QAM are quantum states in a Hilbert space not accessible by classical systems. Hence, comparisons should be done at the same level, either taking a thermodynamic limit of a quantum system and using the classical expression of storage capacity [20], promoting a classical system to the quantum realm and using the expression provided in the main text, or exploiting a relation between the Hilbert space dimension and the size of the

classical system. However, such analysis should be done in a case-by-case basis as is the case for classical spin systems and their quantum generalizations in terms of qubits.

In the case of the classification of classical input data, we can rely on techniques common in quantum machine learning, which use a feature map to encode such data into quantum states [109]. For our approach, and in order to achieve perfect [110] association, it is crucial that data belonging to different labels μ lead to orthogonal decay states $|\omega^{\mu}\rangle$, which then evolve into label states $|\mu\rangle$ (orthogonal or not) [52]. Thus, quantum coding must extract the common features of the μth set that are not found in any other class and encode them in our system of interest [111]. Of course, finding the best feature map is an open problem in the context of quantum machine learning and beyond the scope of this work. Instead, this work reveals the necessary structure that the final channel must have to perform classification tasks.

In conclusion, we have successfully developed a comprehensive framework for QAM using CPTP maps. This framework offers several advantages over classical models, such as the ability to encode non-orthogonal states and potentially store an exponentially large number of patterns efficiently. In our formulation, both classical and quantum patterns can be stored, and such patterns can be either stable or metastable dynamical attractors. We also analyzed the role of symmetries through the definition of basins of attraction, which turn out to be the enabling mechanism for QAM. These findings open up new possibilities for developing more powerful quantum machine learning algorithms, quantum key distribution, and enhanced error correction techniques. Furthermore, they lay the ground to design the most suited implementations on different experimental platforms [21, 23, 25, 27].

Data availability statement

The data that support the findings of this study will be openly available following an embargo at the following URL/DOI: https://gitlab.ifisc.uib-csic.es/quantum/theoretical-framework-for-quantum-associative-memory.

Acknowledgments

We acknowledge the Spanish State Research Agency, through the María de Maeztu project CEX2021-001164-M and through the COQUSY project PID2022-140506NB-C21 and -C22, all funded by MCIU/AEI/10.13039/501100011033; the project is funded under the Quantera II programme that has received funding from the EU's H2020 research and innovation programme under the GA No 101017733, and from the Spanish State Research Agency, PCI2024-153410 funded by MCIU/ AEI/10.13039/5011000 1103; MINECO through the QUANTUM SPAIN Project, and EU through the RTRP—NextGenerationEU within the framework of the Digital Spain 2025 Agenda. ALM is funded by the University of the Balearic Islands through the Project BGRH-UIB-2021. EF acknowledges funding by the European Union's Horizon Europe programme through Grant No. 101105267. GLG is funded by the Spanish Ministerio de Educación y Formación Profesional/Ministerio de Universidades and co-funded by the University of the Balearic Islands through the Beatriz Galindo program (BG20/00085).

Appendix A. HNN

Hopfield originally proposed a network of all-to-all connected binary neurons as a content-addressable memory or AM [2]. Concretely, the model consists of n binary neurons, where the state of the ith neuron, s_i, can take two possible values, $s_i = +1$ and $s_i = -1$, corresponding to the firing and resting states, respectively. The state of the compound system can be represented in terms of a n-bit string $\boldsymbol{s} = (s_1, s_2, \ldots, s_n)$. Further, one can associate the following energy function with the system as follows:

$$E = -\frac{1}{2}\sum_{i\neq j} J_{ij} s_i s_j, \tag{A1}$$

where J_{ij} represent the coupling between the ith and jth neuron. A deterministic dynamics, evolving the state of the system along trajectories that monotonically decrease the energy function, can be defined in terms of the following single flip of the ith neuron:

$$s_i \leftarrow \mathrm{sgn}\left(\sum_{j\neq i} J_{ij} s_j\right). \tag{A2}$$

In the latter, sgn is the sign function, letting the ith neuron fire whenever the input signal coming from the other neurons, $\sum_{j\neq i} J_{ij}s_j$, assumes a positive value. Notice that the input signal plays the role of a local field, $h_i \equiv \sum_{j\neq i} J_{ij}s_j$, acting on the ith neurons. Moreover, the energy function can be expressed in terms of the latter as $E = -\frac{1}{2}\sum_i s_i h_i$. Thus, we can see that at each time step the neuron s_i gets aligned with the local field h_i, and, correspondingly, the energy undergoes a monotonic decrease, eventually reaching a local minimum, i.e. a stable configuration.

The key point is that stable states can be encoded by means of the coupling parameters J_{ij}, in the form of M vectors $\boldsymbol{\xi}^\mu$ representing the patterns. Several rules can be used to encode such memories, the Hebbian learning rule being the most prominent example [1]. Here, the couplings are chosen such that

$$J_{ij} = \frac{1}{n}\sum_{\mu=1}^{M} \xi_i^\mu \xi_j^\mu, \tag{A3}$$

and the patterns are further treated as independent and identically distributed random variables. Their distribution is a bimodal one, with $\mathrm{P}[\xi_i^\mu = \pm 1] = \frac{1}{2}$. As a result, in the large-n limit patterns are unbiased, $\lim_{n\to+\infty}\sum_i \xi_i^\mu/n = 0$, and uncorrelated $\lim_{n\to\infty}\boldsymbol{\xi}^\mu\cdot\boldsymbol{\xi}^\nu/n = \delta^{\mu\nu}$. Under the above conditions, one can show that the patterns $\boldsymbol{\xi}^\mu$ are stable fixed points of the dynamics [112] if $\sqrt{M/n} \ll 1$. In other words, the system behaves as an AM. Indeed, patterns are not only fixed points of the dynamics, but they are also stable ones. This means that for each pattern there exists a basin of attraction, i.e. a finite region of the phase space whose points are asymptotically evolved into the pattern itself.

Hence, an arbitrary initial state $\boldsymbol{s}$ that contains some errors with respect to the patterns is evolved via the dynamics (A2) into the most similar one, thus permitting the retrieval of the correct information. As already commented in the main text, the maximum number of patterns that can be stored by this kind of AM, i.e. its storage capacity, reads $M/n = 0.138$ [30, 31].

It is worth mentioning that the HNN can be further generalized to include some noise, in the form of an effective temperature. The description of the system in this scenario goes beyond the scope of this appendix, and we refer the reader to some literature on the topic [30, 31].

Appendix B. CPTP conditions

A quantum channel is completely positive and trace-preserving if the Kraus operators satisfy the completeness relation (3). Let us enforce this condition for the Kraus operators that are given in the block structure of equation (5). Here, the CPTP condition can be equivalently expressed in terms of the block elements of each Kraus operator, and it reads [51]

$$\sum_\alpha \left(K_\alpha^{\mathrm{S}}\right)^\dagger K_\alpha^{\mathrm{S}} = \mathbb{I}_{\mathrm{S}}, \tag{B1a}$$

$$\sum_\alpha \left(K_\alpha^{\mathrm{S}}\right)^\dagger K_\alpha^{\mathrm{SD}} = \sum_\alpha \left(K_\alpha^{\mathrm{SD}}\right)^\dagger K_\alpha^{\mathrm{S}} = \mathbb{0}_{\mathrm{SD}}, \tag{B1b}$$

$$\sum_\alpha \left(K_\alpha^{\mathrm{SD}}\right)^\dagger K_\alpha^{\mathrm{SD}} + \left(K_\alpha^{\mathrm{D}}\right)^\dagger K_\alpha^{\mathrm{D}} = \mathbb{I}_{\mathrm{D}}. \tag{B1c}$$

In section 4.1 we introduced the form of the Kraus blocks for AM with orthogonal patterns. Using the expression in equation (8)–(10) and substituting in equation (B.1) we find

$$\sum_\mu \sum_j \left[\sum_\alpha |a_{\mu,j}^\alpha|^2\right] |\mu_j\rangle\langle\mu_j| = \mathbb{I}_{\mathrm{S}} \tag{B2a}$$

$$\sum_\mu \sum_j \sum_x \left[\sum_\alpha \left(a_{\mu,j}^\alpha\right)^* b_{\mu,j,x}^\alpha\right] |\mu_j\rangle\langle\mu_j|\omega_x^\mu = \mathbb{0}_{\mathrm{SD}} \tag{B2b}$$

$$\sum_\mu \sum_{x,y=1}^{d_\mu} \left\{\sum_\alpha \left[\sum_j \left(b_{\mu,j,y}^\alpha\right)^* b_{\mu,j,x}^\alpha\right] + \delta_{xy}|c_{\mu,x}|^2\right\} |\omega_x^\mu\rangle\langle\omega_y^\mu| = \mathbb{I}_{\mathrm{D}} \tag{B2c}$$

which reduce to the expressions in equation (11).

When considering non-orthogonal patterns (see section 4.2) we obtain similar results with the addition of an extra index to account for the DFS where the non-orthogonal patterns belong.

Appendix C. Derivation of Kraus parameters

In this section, we derive the form of the parameters that form the Kraus operators in section 4 for the orthogonal and general formulation of the QAM map.

C.1. Orthogonal patterns

Combining equation (11) and (12), we can further express the rate κ^{μ}_{xy} in terms of the coefficients defining the Kraus operators in equation (8)–(10). To do so, as an intermediate step, by exploiting the expressions of $\hat{\rho}_{\mu}$ and $K^{\mathrm{SD}}_{\alpha,\mu}$ (see equation (8)), one can write equation (12) in terms of the following system of equations

$$\sum_{\alpha}\left(b^{\alpha}_{\mu,k,y}\right)^{*} b^{\alpha}_{\mu,j,x} = \kappa^{\mu}_{xy} u^{\mu}_{j}\delta_{jk}. \tag{C1}$$

Thus, by combining the latter with equation (11*c*), the rates κ^{μ}_{xy} read

$$\kappa^{\mu}_{xy} = \delta_{xy}\left[1 - \sum_{\alpha}|c^{\alpha}_{\mu,x}|^{2}\right], \tag{C2}$$

where we must have that $0 < \kappa_{xx} < 1$, whence $\sum_{\alpha}|c_{\mu,x}|^{2} < 1$. Therefore, the rate at which the decaying states are associated with the corresponding pattern is the inverse of the rate at which they vanish, consistently with trace preservation. Finally, plugging the last expression for the rates κ^{μ}_{xy} in the constraint (C1), we obtain the following equation

$$\sum_{\alpha}\left(b^{\alpha}_{\mu,k,y}\right)^{*} b^{\alpha}_{\mu,j,x} = \left[1 - \sum_{\alpha}|c^{\alpha}_{\mu,x}|^{2}\right] u^{\mu}_{j}\delta_{xy}\delta_{jk}. \tag{C3}$$

A simple solution of the latter exists, assuming that there are as many Kraus operators as the number of combinations of (j,x), characterized only by the non-vanishing parameter $b^{(j,k)}_{\mu,j,x}$. If this is the case, we can write

$$b^{\alpha}_{\mu,j,x} = \sqrt{u^{\mu}_{j}\left[1 - \sum_{\alpha}|c^{\alpha}_{\mu,x}|^{2}\right]}\,\delta_{\alpha,j+s_{\mu}x}. \tag{C4}$$

In the above expression, there is no restriction on the choice of the parameters $c^{\alpha}_{\mu,x}$ as long as their modulus-squared sum is smaller than one. In terms of the parameters $a^{\alpha}_{\mu,j}$, we notice that equation (11*b*) imposes a further limit on the Kraus operators displaying $a^{\alpha}_{\mu,j} \neq 0$. Those Kraus operators with a non-zero $b^{\alpha}_{\mu,j,x}$ need to have a vanishing $a^{\alpha}_{\mu,j}$, and vice-versa. Therefore, at least two additional Kraus operators, equipped with a non-vanishing diagonal part of $K^{\mathrm{S}}_{\alpha,\mu}$, need to exist.

Notice that the solution obtained in equation (C4) corresponds to the configuration requiring the least amount of Kraus operators. However, such a solution is not unique, as by increasing the number of Kraus operators, one can find other maps Λ satisfying the constraints. To conclude, we stress that the parameters $a^{\alpha}_{\mu,j}$, $b^{\alpha}_{\mu,j,x}$ and $c^{\alpha}_{\mu,x}$ can be considered as degrees of freedom that can be tuned to guarantee the associativity condition defined by equation (6).

C.2. General formulation

Similar to the previous case, we can find an expression for the mixing parameters for Kraus operators acting on DFS. Substituting equation (17) in equation (18), we obtain

$$\sum_{\alpha}(b^{\alpha,\tau}_{\ell',k,y})^{*} b^{\alpha,\tau}_{\ell,j,x} = \delta_{\ell\ell'}\kappa^{\ell}_{xy}\langle\tau_{j}|\hat{\rho}^{(\tau)}_{\ell}|\tau_{k}\rangle. \tag{C5}$$

By combining equation (17) and equation (16), the CPTP condition (B1*c*) (see appendix B) reads

$$\sum_{\alpha}\left[\sum_{j=1}^{s_{\tau}}\left(b^{\alpha,\tau}_{\ell',j,y}\right)^{*} b^{\alpha,\tau}_{\ell,j,x}\right] + \delta_{\ell\ell'}\delta_{xy}|c^{\alpha,\tau}_{\ell,x}|^{2} = \delta_{\ell\ell'}\delta_{xy}. \tag{C6}$$

Thus, similarly to the derivation of equation (C2), an expression for the rate parameters κ^{ℓ}_{xy} can be obtained. Substituting equation (C5) into equation (C6), we get

$$\kappa^{\ell}_{xy} = \delta_{xy}\left[1 - \sum_{\alpha}|c^{\alpha,\tau}_{\ell,x}|^{2}\right], \tag{C7}$$

and the expression for the mixing parameters reads

$$\sum_{\alpha}\left(b^{\alpha,\tau}_{\ell',k,y}\right)^{*} b^{\alpha,\tau}_{\ell,j,x}=\delta_{\ell\ell'}\delta_{xy}\left[1-\sum_{\alpha}|c^{\alpha,\tau}_{\ell,x}|^{2}\right]\langle\tau_j|\hat{\rho}^{(\tau)}_{\ell}|\tau_k\rangle. \tag{C8}$$

For the particular case $\hat{\rho}^{(\tau)}_{\ell}=|\psi^{(\tau)}_{\ell}\rangle\langle\psi^{(\tau)}_{\ell}|$ where $|\psi^{(\tau)}_{\ell}\rangle=\sum_{j=1}^{s_\tau}[\psi^{(\tau)}_{\ell}]_j|\tau_j\rangle$ we may find a solution

$$b^{\alpha,\tau}_{\ell,j,x}=\left[\psi^{(\tau)}_{\ell}\right]_j\sqrt{1-\sum_{\alpha}|c^{\alpha}_{\tau,x}|^{2}}\,\delta_{\alpha-\alpha_0,xm^{\max}_{\not\perp}+\ell}. \tag{C9}$$

with $m^{\max}_{\not\perp}=\max_\tau m^{(\tau)}_{\not\perp}$ and α_0 is the number of Kraus operators with non-vanishing elements in the stable and decaying part ($\alpha_0\in[2,(N^{\mathrm{S}})^2+(N^{\mathrm{D}})^2]$). The index of the Kraus operators runs over $\alpha=1,\ldots,m^{\not\perp}_{\max}d_{\max}$ where $d_{\max}=\max_\tau d^{(\tau)}_{\ell}$ since parameters belonging to different $\mathcal{X}_\tau$ and different $\mathcal{S}_\mu$ can go in the same Kraus as they are not restricted by the CPTP conditions.

Appendix D. Relation with genuine incoherent operation

In this work, we emphasize the necessity that QAM feature non-empty decaying subspace, $\mathcal{D}$. In this way, the states belonging to the latter can be associated with the patterns, i.e. states of the invariant subspace $\mathcal{S}$, via the dynamical maps of section 4. In this appendix, we show how such a framework can encompass a model previously proposed [28, 62], in which a CPTP map is derived displaying multiple fixed points. Notably, and at variance with our construction, such a map stores an entire basis of the Hilbert space as patterns. Hence, in our formalism, this scenario corresponds to the entire Hilbert space being the stable space, $\mathcal{S}=\mathcal{H}$, leaving an empty decaying space $\mathcal{D}=\emptyset$. In fact, as we show in the following, it is possible to derive the above-commented
map as a particular case of the QAM that we obtained in section 4.1.

Let $\{|\mu\rangle\}$ represent a basis of the Hilbert space, with each state $|\mu\rangle$ being invariant under the map Λ. According to equation (8), the Kraus operators read

$$K^{\mathrm{S}}_{\alpha}=K_\alpha=\sum_{\mu}a^{\alpha}_{\mu}|\mu\rangle\langle\mu|, \tag{D1}$$

which, by assumption, defines the Kraus operator acting on the whole Hilbert space $\mathcal{H}$. In the Jamiolkowski–Choi–Sudarshan (JCS) representation [113], the map Λ can be expressed in terms of the following linear operator

$$J_\Lambda=\sum_{\alpha}|K_\alpha\rangle\rangle\langle\langle K_\alpha|, \tag{D2}$$

such that $J_\Lambda\in\mathcal{B}(\mathcal{H}\otimes\mathcal{H})$, and where we have also introduced

$$|K_\alpha\rangle\rangle=\sum_{\mu}a^{\alpha}_{\mu}|\mu\mu\rangle\rangle, \tag{D3}$$

with $|\mu\mu\rangle\rangle\in\mathcal{H}\otimes\mathcal{H}$. By plugging the above in the JCS representation of the map, we obtain

$$\begin{aligned}J_\Lambda&=\sum_{\alpha}\sum_{\mu,\nu}(a^{\alpha}_{\nu})^{*}a^{\alpha}_{\mu}|\mu\mu\rangle\rangle\langle\langle\nu\nu|\\&=\sum_{\mu}|\mu\mu\rangle\rangle\langle\langle\mu\mu|+\sum_{\mu\neq\nu}\left[\sum_{\alpha}(a^{\alpha}_{\nu})^{*}a^{\alpha}_{\mu}\right]|\mu\mu\rangle\rangle\langle\langle\nu\nu|,\end{aligned} \tag{D4}$$

having further employed the CPTP condition of the Kraus operators (equation (B1*a*)) in the second line. Identifying the term in square brackets with coefficients of the form $1+\gamma_{\mu\nu}$ we recover the expression of the map proposed [28]. Moreover, being the spectral radius of CPTP maps bounded by 1, so that $|a^{\alpha}_{\mu}|\leqslant 1$, we obtain $|1+\gamma_{\mu\nu}|\leqslant 1$ if $a^{\alpha}_{\mu}\neq a^{\alpha}_{\nu}$, this leading to vanishing coherences upon many repetition of the map.

ORCID iDs

Adrià Labay-Mora https://orcid.org/0000-0002-3443-4929
Eliana Fiorelli https://orcid.org/0000-0003-4677-3204
Roberta Zambrini https://orcid.org/0000-0002-9896-3563
Gian Luca Giorgi https://orcid.org/0000-0003-3113-0193

References

[1] Hebb D O 2005 *The Organization of Behavior: A Neuropsychological Theory* (Psychology Press)
[2] Hopfield J J 1982 Neural networks and physical systems with emergent collective computational abilities *Proc. Natl Acad. Sci.* **79** 2554
[3] Jaeger R C, Blalock T N and Blalock B J 1997 *Microelectronic Circuit Design* vol 97 (McGraw-Hill)
[4] Zhang G P 2000 Neural networks for classification: a survey *IEEE Trans. Syst. Man Cybern. C* **30** 451
[5] Biamonte J, Wittek P, Pancotti N, Rebentrost P, Wiebe N and Lloyd S 2017 Quantum machine learning *Nature* **549** 195
[6] Cerezo M, Verdon G, Huang H-Y, Cincio L and Coles P J 2022 Challenges and opportunities in quantum machine learning *Nat. Comput. Sci.* **2** 567
[7] Ventura D and Martinez T 2000 Quantum associative memory *Inf. Sci.* **124** 273
[8] Trugenberger C A 2001 Probabilistic quantum memories *Phys. Rev. Lett.* **87** 067901
[9] Diamantini M C and Trugenberger C A 2006 Quantum pattern retrieval by qubit networks with Hebb interactions *Phys. Rev. Lett.* **97** 130503
[10] Cao Y, Guerreschi G G and Aspuru-Guzik A 2017 Quantum neuron: an elementary building block for machine learning on quantum computers (arXiv:1711.11240)
[11] Miller N E and Mukhopadhyay S 2021 A quantum Hopfield associative memory implemented on an actual quantum processor *Sci. Rep.* **11** 23391
[12] Quiroz G, Ice L, Delgado A and Humble T S 2021 Particle track classification using quantum associative memory *Nucl. Instrum. Methods Phys. Res. A* **1010** 165557
[13] Rebentrost P, Bromley T R, Weedbrook C and Lloyd S 2018 Quantum Hopfield neural network *Phys. Rev. A* **98** 042308
[14] Inoue J-i 2011 Pattern-recalling processes in quantum Hopfield networks far from saturation *J. Phys.: Conf. Ser.* **297** 012012
[15] Neigovzen R, Neves J L, Sollacher R and Glaser S J 2009 Quantum pattern recognition with liquid-state nuclear magnetic resonance *Phys. Rev. A* **79** 042321
[16] Das S, Zhang J, Martina S, Suter D and Caruso F 2023 Quantum pattern recognition on real quantum processing units *Quantum Mach. Intell.* **5** 16
[17] Rotondo P, Marcuzzi M, Garrahan J P, Lesanovsky I and Müller M 2018 Open quantum generalisation of Hopfield neural networks *J. Phys. A: Math. Theor.* **51** 115301
[18] Fiorelli E, Rotondo P, Marcuzzi M, Garrahan J P and Lesanovsky I 2019 Quantum accelerated approach to the thermal state of classical all-to-all connected spin systems with applications to pattern retrieval in the Hopfield neural network *Phys. Rev. A* **99** 032126
[19] Fiorelli E, Lesanovsky I and Müller M 2022 Phase diagram of quantum generalized Potts-Hopfield neural networks *New J. Phys.* **24** 033012
[20] Bödeker L, Fiorelli E and Müller M 2023 Optimal storage capacity of quantum Hopfield neural networks *Phys. Rev. Res.* **5** 023074
[21] Fiorelli E, Marcuzzi M, Rotondo P, Carollo F and Lesanovsky I 2020 Signatures of associative memory behavior in a multimode Dicke model *Phys. Rev. Lett.* **125** 070604
[22] Carollo F and Lesanovsky I 2021 Exactness of mean-field equations for open Dicke models with an application to pattern retrieval dynamics *Phys. Rev. Lett.* **126** 230601
[23] Marsh B P, Guo Y, Kroeze R M, Gopalakrishnan S, Ganguli S, Keeling J and Lev B L 2021 Enhancing associative memory recall and storage capacity using confocal cavity QED *Phys. Rev. X* **11** 021048
[24] Schuld M, Sinayskiy I and Petruccione F 2014 Quantum walks on graphs representing the firing patterns of a quantum neural network *Phys. Rev. A* **89** 032333
[25] Tang H *et al* 2019 Experimental quantum stochastic walks simulating associative memory of Hopfield neural networks *Phys. Rev. Appl.* **11** 024020
[26] Labay-Mora A, Zambrini R and Giorgi G L 2023 Quantum associative memory with a single driven-dissipative nonlinear oscillator *Phys. Rev. Lett.* **130** 190602
[27] Labay-Mora A, Zambrini R and Giorgi G L 2024 Quantum memories for squeezed and coherent superpositions in a driven-dissipative nonlinear oscillator *Phys. Rev. A* **109** 032407
[28] Lewenstein M, Gratsea A, Riera-Campeny A, Aloy A, Kasper V and Sanpera A 2021 Storage capacity and learning capability of quantum neural networks *Quantum Sci. Technol.* **6** 045002
[29] Macieszczak K, Rose D C, Lesanovsky I and Garrahan J P 2021 Theory of classical metastability in open quantum systems *Phys. Rev. Res.* **3** 033047
[30] Amit D J, Gutfreund H and Sompolinsky H 1985 Spin-glass models of neural networks *Phys. Rev. A* **32** 1007
[31] Amit D J, Gutfreund H and Sompolinsky H 1985 Storing infinite numbers of patterns in a spin-glass model of neural networks *Phys. Rev. Lett.* **55** 1530
[32] McEliece R, Posner E, Rodemich E and Venkatesh S 1987 The capacity of the Hopfield associative memory *IEEE Trans. Inf. Theory* **33** 461
[33] Demircigil M, Heusel J, Löwe M, Upgang S and Vermet F 2017 On a model of associative memory with huge storage capacity *J. Stat. Phys.* **168** 288
[34] Willshaw D J, Buneman O P and Longuet-Higgens H C 1969 Non-holographic associative memory *Nature* **222** 960
[35] Gardner E and Derrida B 1988 Optimal storage properties of neural network models *J. Phys. A: Math. Gen.* **21** 271
[36] Gardner E 1988 The space of interactions in neural network models *J. Phys. A: Math. Gen.* **21** 257
[37] Wolf M M 2012 Quantum channels and operations-guided tour
[38] Breuer H-P and Petruccione F 2002 *The Theory of Open Quantum Systems* (Oxford University Press)
[39] Nielsen M A and Chuang I L 2010 *Quantum Computation and Quantum Information* (Cambridge University Press)
[40] In this work, we will focus on completely positive trace-preserving (CPTP) channels that map elements of $\mathcal{B}(\mathcal{H})$ to itself.
[41] Kraus K, Böhm A, Dollard J D and Wootters W 1983 *States, Effects and Operations Fundamental Notions of Quantum Theory: Lectures in Mathematical Physics at the University of Texas at Austin* (Springer)
[42] Arias A, Gheondea A and Gudder S P 2002 Fixed points of quantum operations *J. Math. Phys.* **43** 5872
[43] Watrous J 2018 *The Theory of Quantum Information* (Cambridge University Press)
[44] Evans D E and Hanche-Olsen H 1979 The generators of positive semigroups *J. Funct. Anal.* **32** 207
[45] Burgarth D, Chiribella G, Giovannetti V, Perinotti P and Yuasa K 2013 Ergodic and mixing quantum channels in finite dimensions *New J. Phys.* **15** 073045

[46] Baumgartner B and Narnhofer H 2012 The structures of state space concerning quantum dynamical semigroups *Rev. Math. Phys.* **24** 1250001
[47] Carbone R and Pautrat Y 2016 Irreducible decompositions and stationary states of quantum channels *Rep. Math. Phys.* **77** 293
[48] More precisely, for semigroup of quantum maps, both in discrete time and continuous one
[49] Defining $P_{\mathcal{S}}$ the projector onto the invariant subspace $\mathcal{S}$, the map is attractive if $lim_{r\to\infty}\Lambda^{r,\dagger}(P_{\mathcal{S}})$ converges to 1 in expectation value. See [50] for a rigorous definition
[50] Carbone R and Girotti F 2021 Absorption in invariant domains for semigroups of quantum channels *Ann. Henri Poincaré* **22** 2497
[51] Albert V V 2019 Asymptotics of quantum channels: conserved quantities, an adiabatic limit and matrix product states *Quantum* **3** 151
[52] Marshall J, Campos Venuti L and Zanardi P 2019 Classifying quantum data by dissipation *Phys. Rev. A* **99** 032330
[53] Schuld M, Sinayskiy I and Petruccione F 2014 The quest for a quantum neural network *Quantum Inf. Process.* **13** 2567
[54] Ramsauer H et al 2020 Hopfield networks is all you need (arXiv:2008.02217)
[55] Buča B and Prosen T 2012 A note on symmetry reductions of the lindblad equation: transport in constrained open spin chains *New J. Phys.* **14** 073007
[56] Albert V V and Jiang L 2014 Symmetries and conserved quantities in lindblad master equations *Phys. Rev. A* **89** 022118
[57] Minganti F, Biella A, Bartolo N and Ciuti C 2018 Spectral theory of Liouvillians for dissipative phase transitions *Phys. Rev. A* **98** 042118
[58] Strogatz S H 2018 *Nonlinear Dynamics and Chaos: With Applications to Physics, Biology, Chemistry and Engineering* (CRC Press)
[59] Torres J J and Manzano D 2023 Dissipative quantum Hopfield network: a numerical analysis *New J. Phys.* **26** 103018
[60] Schuld M, Sinayskiy I and Petruccione F 2014 Quantum computing for pattern classification *PRICAI 2014: Trends in Artificial Intelligence: 13th Pacific Rim Int. Conf. on Artificial Intelligence (Gold Coast, QLD, Australia, 1–5 December 2014. Proc. 13)* (Springer) pp 208–20
[61] The map restricted to each basin of attraction $\mathcal{S}_\mu$ is irreducible
[62] Marconi C, Saus P C, Díaz M G and Sanpera A 2022 The role of coherence theory in attractor quantum neural networks *Quantum* **6** 794
[63] de Vicente J I and Streltsov A 2016 Genuine quantum coherence *J. Phys. A: Math. Theor.* **50** 045301
[64] Amato D, Facchi P and Konderak A 2023 Asymptotics of quantum channels *J. Phys. A: Math. Theor.* **56** 265304
[65] Little W and Shaw G L 1978 Analytic study of the memory storage capacity of a neural network *Math. Biosci.* **39** 281
[66] Chefles A 2000 Quantum state discrimination *Contemp. Phys.* **41** 401
[67] Bergou J A 2010 Discrimination of quantum states *J. Mod. Opt.* **57** 160
[68] Helstrom C W 1969 Quantum detection and estimation theory *J. Stat. Phys.* **1** 231
[69] Rudolph T, Spekkens R W and Turner P S 2003 Unambiguous discrimination of mixed states *Phys. Rev. A* **68** 010301(R)
[70] Dalla Pozza N and Pierobon G 2015 Optimality of square-root measurements in quantum state discrimination *Phys. Rev. A* **91** 042334
[71] Ban M, Kurokawa K, Momose R and Hirota O 1997 Optimum measurements for discrimination among symmetric quantum states and parameter estimation *Int. J. Theor. Phys.* **36** 1269
[72] Eldar Y and Forney G 2001 On quantum detection and the square-root measurement *IEEE Trans. Inf. Theory* **47** 858
[73] Blume-Kohout R, Ng H K, Poulin D and Viola L 2010 Information-preserving structures: a general framework for quantum zero-error information *Phys. Rev. A* **82** 062306
[74] Macieszczak K, Guta M, Lesanovsky I and Garrahan J P 2016 Towards a theory of metastability in open quantum dynamics *Phys. Rev. Lett.* **116** 240404
[75] Minganti F, Savona V and Biella A 2023 Dissipative phase transitions in n-photon driven quantum nonlinear resonators *Quantum* **7** 1170
[76] Mirrahimi M, Leghtas Z, Albert V V, Touzard S, Schoelkopf R J, Jiang L and Devoret M H 2014 Dynamically protected cat-qubits: a new paradigm for universal quantum computation *New J. Phys.* **16** 045014
[77] Mundhada S O, Grimm A, Touzard S, Vool U, Shankar S, Devoret M H and Mirrahimi M 2017 Generating higher-order quantum dissipation from lower-order parametric processes *Quantum Sci. Technol.* **2** 024005
[78] Gevorkyan S and Chaltykyan V 1999 Coherent superposition states of light and their interference in three-photon absorption process *J. Mod. Opt.* **46** 1447
[79] Braunstein S L and McLachlan R I 1987 Generalized squeezing *Phys. Rev. A* **35** 1659
[80] Lang B and Armour A D 2021 Multi-photon resonances in Josephson junction-cavity circuits *New J. Phys.* **23** 033021
[81] Xuan Q D, Zhang Z and Voss P L 2009 A 24 km fiber-based discretely signaled continuous variable quantum key distribution system *Opt. Express* **17** 24244
[82] Lin J, Upadhyaya T and Lütkenhaus N 2019 Asymptotic security analysis of discrete-modulated continuous-variable quantum key distribution *Phys. Rev. X* **9** 041064
[83] The POVM is completed by the unambiguous operator $\Pi_? = \mathbb{I} - \sum_\mu \Pi_\mu$ which triggers with a small probability if the lobes are approximately orthogonal, in such case the state is unclassified
[84] Lieu S, Belyansky R, Young J T, Lundgren R, Albert V V and Gorshkov A V 2020 Symmetry breaking and error correction in open quantum systems *Phys. Rev. Lett.* **125** 240405
[85] Vlastakis B, Kirchmair G, Leghtas Z, Nigg S E, Frunzio L, Girvin S M, Mirrahimi M, Devoret M H and Schoelkopf R J 2013 Deterministically encoding quantum information using 100-photon schrödinger cat states *Science* **342** 607
[86] Bergmann M and van Loock P 2016 Quantum error correction against photon loss using multicomponent cat states *Phys. Rev. A* **94** 042332
[87] The particular case $M = 2$ leads to orthogonal patterns which fall into a similar case of section 8.1
[88] Grover L K 2005 Fixed-point quantum search *Phys. Rev. Lett.* **95** 150501
[89] Tulsi T, Grover L K and Patel A 2005 A new algorithm for fixed point quantum search (arXiv:0505007)
[90] Yoder T J, Low G H and Chuang I L 2014 Fixed-point quantum search with an optimal number of queries *Phys. Rev. Lett.* **113** 210501
[91] Brun T, Klauck H, Nayak A, Rötteler M and Zalka C 2003 Comment on 'probabilistic quantum memories' *Phys. Rev. Lett.* **91** 209801
[92] Trugenberger C A 2003 Trugenberger replies: *Phys. Rev. Lett.* **91** 209802
[93] Fiorelli E, Müller M, Lesanovsky I and Carollo F 2023 Mean-field dynamics of open quantum systems with collective operator-valued rates: validity and application *New J. Phys.* **25** 083010

[94] Sannia A, Martínez-Peña R, Soriano M C, Giorgi G L and Zambrini R 2024 Dissipation as a resource for quantum reservoir computing *Quantum* **8** 1291
[95] Kubota T, Suzuki Y, Kobayashi S, Tran Q H, Yamamoto N and Nakajima K 2023 Temporal information processing induced by quantum noise *Phys. Rev. Res.* **5** 023057
[96] Beer K, Bondarenko D, Farrelly T, Osborne T J, Salzmann R, Scheiermann D and Wolf R 2020 Training deep quantum neural networks *Nat. Commun.* **11** 808
[97] Mele A A, Angrisani A, Ghosh S, Khatri S, Eisert J, França D S and Quek Y 2024 Noise-induced shallow circuits and absence of barren plateaus (arXiv:2403.13927)
[98] Sannia A, Tacchino F, Tavernelli I, Giorgi G L and Zambrini R 2024 Engineered dissipation to mitigate barren plateaus *npj Quantum Inf.* **10** 81
[99] Mi X *et al* 2024 Stable quantum-correlated many-body states through engineered dissipation *Science* **383** 1332–7
[100] Krauter H, Muschik C A, Jensen K, Wasilewski W, Petersen J M, Cirac J I and Polzik E S 2011 Entanglement generated by dissipation and steady state entanglement of two macroscopic objects *Phys. Rev. Lett.* **107** 080503
[101] Gravina L, Minganti F and Savona V 2023 Critical Schrödinger cat qubit *PRX Quantum* **4** 020337
[102] Gertler J M, Baker B, Li J, Shirol S, Koch J and Wang C 2021 Protecting a bosonic qubit with autonomous quantum error correction *Nature* **590** 243
[103] Cattaneo M, De Chiara G, Maniscalco S, Zambrini R and Giorgi G L 2021 Collision models can efficiently simulate any multipartite markovian quantum dynamics *Phys. Rev. Lett.* **126** 130403
[104] Cattaneo M, Rossi M A C, García-Pérez G, Zambrini R and Maniscalco S 2023 Quantum simulation of dissipative collective effects on noisy quantum computers *PRX Quantum* **4** 010324
[105] Verstraete F, Wolf M M and Ignacio Cirac J 2009 Quantum computation and quantum-state engineering driven by dissipation *Nat. Phys.* **5** 633
[106] Larocca M, Sauvage F, Sbahi F M, Verdon G, Coles P J and Cerezo M 2022 Group-invariant quantum machine learning *PRX Quantum* **3** 030341
[107] Nguyen Q T, Schatzki L, Braccia P, Ragone M, Coles P J, Sauvage F, Larocca M and Cerezo M 2024 Theory for equivariant quantum neural networks *PRX Quantum* **5** 020328
[108] Meyer J J, Mularski M, Gil-Fuster E, Mele A A, Arzani F, Wilms A and Eisert J 2023 Exploiting symmetry in variational quantum machine learning *PRX Quantum* **4** 010328
[109] Schuld M and Killoran N 2019 Quantum machine learning in feature Hilbert spaces *Phys. Rev. Lett.* **122** 040504
[110] Here, we refer to perfect classification as the fact that an input belonging entirely to a class will, at the end of the association process, have components only in the quantum state of that class
[111] Lloyd S, Schuld M, Ijaz A, Izaac J and Killoran N 2020 Quantum embeddings for machine learning (arXiv:2001.03622)
[112] In fact, also the antipatterns $-\boldsymbol{\xi}^{\mu}$ are stable local minima, and there appear $2M$ configurations that minimize the energy. This is a straightforward consequence of the $\mathbb{Z}_2$ symmetry characterizing the energy function
[113] Choi M-D 1975 Completely positive linear maps on complex matrices *Linear Algebr. Appl.* **10** 285